

ACCEPTED MANUSCRIPT

Advances in volumetric bioprinting

To cite this article before publication: Sibó Jíng *et al* 2023 *Biofabrication* in press <https://doi.org/10.1088/1758-5090/ad0978>

Manuscript version: Accepted Manuscript

Accepted Manuscript is “the version of the article accepted for publication including all changes made as a result of the peer review process, and which may also include the addition to the article by IOP Publishing of a header, an article ID, a cover sheet and/or an ‘Accepted Manuscript’ watermark, but excluding any other editing, typesetting or other changes made by IOP Publishing and/or its licensors”

This Accepted Manuscript is © 2023 IOP Publishing Ltd.



During the embargo period (the 12 month period from the publication of the Version of Record of this article), the Accepted Manuscript is fully protected by copyright and cannot be reused or reposted elsewhere.

As the Version of Record of this article is going to be / has been published on a subscription basis, this Accepted Manuscript will be available for reuse under a CC BY-NC-ND 3.0 licence after the 12 month embargo period.

After the embargo period, everyone is permitted to use copy and redistribute this article for non-commercial purposes only, provided that they adhere to all the terms of the licence <https://creativecommons.org/licenses/by-nc-nd/3.0>

Although reasonable endeavours have been taken to obtain all necessary permissions from third parties to include their copyrighted content within this article, their full citation and copyright line may not be present in this Accepted Manuscript version. Before using any content from this article, please refer to the Version of Record on IOPscience once published for full citation and copyright details, as permissions may be required. All third party content is fully copyright protected, unless specifically stated otherwise in the figure caption in the Version of Record.

View the [article online](#) for updates and enhancements.

Advances in Volumetric Bioprinting

Sibo Jing,^{1,#} Liming Lian,^{2,#} Yingying Hou,^{1,#} Zeqing Li,¹ Zihao Zheng,¹ Gang Li,³ Guosheng Tang,^{4,*} Guoxi Xie,^{1,*} and Maobin Xie^{1,2,*}

¹The Sixth Affiliated Hospital of Guangzhou Medical University, Qingyuan People's Hospital; Guangzhou Municipal and Guangdong Provincial Key Laboratory of Protein Modification and Degradation; School of Biomedical Engineering, Guangzhou Medical University, Guangzhou 511436, P. R. China.

²Wallace H. Coulter Department of Biomedical Engineering, Georgia Institute of Technology, Atlanta, GA 30332, USA.

³National Engineering Laboratory for Modern Silk; College of Textile and Clothing Engineering, Soochow University, Suzhou 215123, China.

⁴Guangzhou Municipal and Guangdong Provincial Key Laboratory of Molecular Target & Clinical Pharmacology, the NMPA and State Key Laboratory of Respiratory Disease, School of Pharmaceutical Sciences and the Fifth Affiliated Hospital, Guangzhou Medical University, Guangzhou 511436, P. R. China.

*Author to whom correspondence should be addressed: maobinxie@gzhmu.edu.cn (M. B. Xie); guoxixie@163.com (G. X. Xie); guoshengtang@gzhmu.edu.cn (G. S. Tang)

Abstract

The three-dimensional (3D) bioprinting technologies are suitable for biomedical applications owing to their ability to manufacture complex and high-precision tissue constructs. However, the slow printing speed of current layer-by-layer (bio)printing modality is the major limitation in biofabrication field. To overcome this issue, volumetric bioprinting (VBP) is developed. VBP changes the layer-wise operation of conventional devices, permitting the creation of geometrically complex, centimeter-scale constructs in tens of seconds. VBP is the next step onward from sequential biofabrication methods, opening new avenues for fast additive manufacturing (AM) in the fields of tissue engineering, regenerative medicine, personalized drug testing, and soft robotics, etc. Therefore, this review introduces the printing principles and hardware designs of VBP-based techniques; then focuses on the recent advances in VBP-based (bio)inks and their biomedical applications. Lastly, the current limitations of VBP are discussed together with future direction of research.

Keywords: volumetric bioprinting; biofabrication; (bio)ink; biomedical application

1. Introduction

Bioprinting is an evolving research field, which attracts attentions from tissue engineering, regenerative medicine, personalized drug testing etc [1]-[3]. Normally, three-dimensional printing (3DP) equipment and bioinks are used to complete bioprinting process. Bioprinting is an interdisciplinary technology that integrates materials science, mechanical design, computer science, and optics [4],[5]. 3DP can be divided into four categories (**figure 1**): 0D (point-at-once): inkjet-based bioprinting [6]-[10]; 1D (line-at-once): extrusion-based bioprinting [11]-[19]; 2D (layer-at-once): digital light processing (DLP) [20]-[26], continuous liquid interface printing (CLIP) [27] and injection continuous liquid interface production (iCLIP) [28]; 3D (volume-at-once): computed axial lithography (CAL) [29], which is an emerging 3D (bio)printing paradigm that can print all points of the objects at the same time. The major limitations of traditional bioprinting technologies are slow printing speed and poor surface quality [30]. Vat photopolymerization offers a faster printing speed and a better printing performance by selectively curing light-activated polymer in the vat compares to FDM [31]. However, the commonly used ultraviolet (UV) light source in vat photopolymerization process would damage cells, which poses significant obstacles for bioprinting and the following biomedical applications. CAL technology enables printing centimeter-level objects within 30-300 s and resulting a high cell viability, showing great potentials in bioprinting.

The concept of bioprinting is to print with living materials such as cells or bacteria to build biomimetic 3D tissues [32]. The bioprinting process includes three key elements: (1) bioprinting technology; (2) bioinks; (3) post-treatment and culturing of 3D living constructs. Long bioprinting time of traditional 3DP would cause stress to cells and compromise cell viability when exposing them in external environment [33],[34]. In contrast, the visible light-activated volumetric bioprinting (VBP) technology could (bio)print sophisticate constructs at a centimeter scale within tens of seconds, which avoids using UV light or high temperature during bioprinting process as well, showing a great potential in biofabrication [35].

1
2
3
4 In addition, bioinks play an important role in bioprinting as well, due to the physicochemical
5 properties of bioinks would significantly influence the printing fidelity, cell viability and functions
6 [36],[37]. Notably, compared with bioinks used in traditional layer-by-layer bioprinting
7 technologies, the bioinks used in VBP could be used at ultra-low concentrations, which broadens
8 choices and expanding the bioink bank. However, the bioinks for VBP still have some special
9 requirements, such as excellent light penetration performance and appropriate viscosity [79].
10
11

12
13
14
15 In this review, the recent development of VBP and related technologies in terms of their
16 working rationale and hardware designs are summarized. Then we focus on the advances in
17 (bio)inks for VBP, followed by further discussion of their biomedical applications. At last, the
18 limitations and future directions of VBP are discussed. **Table 1** provides a list of abbreviations
19 used in this review.
20
21
22
23
24

25 **2. Printing principle and instrumental design of VBP**

26
27 The concept of VBP was first proposed by Shusteff *et al* group in 2017, which was inspired by
28 holography (**figure 2(A)**). It projected beams from three directions to the resin to cure the
29 photopolymer simultaneously [38]. Then, Taylor *et al* group drew inspiration from the image
30 reconstruction procedure of computed tomography (CT) and developed computed axial
31 lithography (CAL) system to fabricate 3D parts (**figure 2(B)**) [39],[40]. In 2020, Loterie *et al* group
32 designed an integrated feedback system to improve the printing resolution of CAL (**figure 2(C)**),
33 which could produce centimeter-scale structures with 80- μm positive resolution and 500- μm
34 negative resolution within 30 s [41]. Xolography, the linear volumetric 3DP system (**figure 2(D)**),
35 is different from the previous volumetric systems, uses a dual beam to cure photoresin and achieve
36 a resolution approximately ten times higher than CAL [42].
37
38
39
40
41
42
43
44
45
46

47 **2.1. Computed axial lithography system for (bio)printing**

48
49 In 2019, Taylor *et al* group developed a CAL technology [39], which includes three components:
50 a light source, a platform, and a rotational vial (**figure 3(A)**). The principle of CAL technology is
51 inspired by the computed tomography (CT) image reconstruction procedure. At the time of
52 printing, DLP projects a set of 2D images from different angles into the synchronized rotating resin
53
54
55
56
57
58
59
60

1
2
3
4 container. The photosensitive resin would solidify at the designed position after obtaining
5 superimposed illumination from multiple angles. The physical setup system consists of three main
6 parts: DLP projector [43], lens, and printing platform. The printing platform consists of a
7 cylindrical glass vial (1-5 cm in diameter) and a stepper motor. The motor would rotate the
8 cylindrical glass vial at a rotation rate of 3-25 degrees per second while printing. This system could
9 fabricate centimeter-level constructs within 30-300 s. There are six steps to do to print an ideal
10 model, for example, *The Thinker* (**figure 3(B)**): (i) imports the standard stereolithography file
11 format (.stl) and slices the target geometry $f_t(r,z)$ (**figure 3(C)**); (ii) the inverse Radon transform
12 (**figure 3(D)**) and Fourier transform (**figure 3(E)**) algorithms are used to compute projection
13 intensities of each z slice; (iii) high pass back-projection filter algorithm is applied to truncate
14 negative information; (iv) the heuristic algorithm is used to iterative optimization projection
15 images to make printed geometry $f(r,z)$ closely simulate the desired target geometry $f_T(r,z)$; (v)
16 the optimized images are projected into photoresin container; (vi) completes the printing and rinses
17 out the construct.
18
19
20
21
22
23
24
25
26
27
28
29
30

31 **2.2. High-resolution volumetric manufacturing system for (bio)printing**

32
33 To improve the (bio)printing resolution and stability of CAL, Loterie *et al* group designed a high-
34 resolution VBP system (**figure 2(C)**) [41]. The printing principle is similar to CAL system. The
35 main difference between high-resolution VBP system and CAL system is the addition of a
36 feedback system, which can image the (bio)printing process and accurately control the next
37 (bio)printing process. In detail, a camera was placed at a 90° relative to the projection direction to
38 record the formation of target object in the vial. The first recorded images were used to adjust
39 exposure time and intensity in the second-time (bio)printing process. The obtained construct could
40 achieve a positive feature of 80 um and a negative feature of 500 um through this correction [41].
41 The optimization process needs seven steps (**figure 4(A)**): (i) a camera was used to record the
42 (bio)printing images (**figure 4(B)**) of pro-exposure resin vial and defined as $I_{bg}(x',z',\theta)$, which
43 was crucial for next optimal computation; (ii) recording the corresponding angle of each image
44
45
46
47
48
49
50
51
52
53
54
55
56
57
58
59
60

during exposure and defined as $I_{rec}(x',z',\theta,n)$; (iii) calculating the difference of recordings during exposure and background images:

$$I_{diff}(x',z',\theta,n) = I_{bg}(x',z',\theta) - I_{rec}(x',z',\theta,n) \quad (1)$$

(iv) Setting threshold $T = \frac{1}{3} \max I_{diff}$ to detect changes compared to empty vial images:

$$I_{thresh}(x',z',\theta,n) = \begin{cases} 1 & \text{if } I_{diff}(x',z',\theta,n) > T \\ 0 & \text{elsewhere} \end{cases} \quad (2)$$

(v) Arranging exposure images in chronological order and finding out the time and angle of over-cured and uncured successfully:

$$t_{poly}(x',z',\theta) = \min_n \{t(n,0) | \forall n' \geq n: I_{thresh}(x',z',\theta,n')\} \quad (3)$$

(vi) Using following formula to back-projection polymerization times in 3D:

$$t_{3D}(x,y,z) = \max_{\theta} \{t_{poly}(x \cos \theta - y \sin \theta, z, \tan^{-1}(y,x))\} \quad (4)$$

(vii) Using the map of the polymerization times to modulate voxels that increase or decrease dosage in time and position of uncured or over-cured in next printing process. Finally, a mouse pulmonary artery model (**figure 4(C)**) and a hearing aid shell model (**figure 4(D)**) was printed to verify the performance of the feedback system.

Further, Antony Orth *et al* group used a new imaging modality called optical scattering tomography (OST) in VBP, which could visualize and quantitatively measure the (bio)printing constructs [44]. Their work paves a way for real-time defect detection and correction of high-fidelity tissues and organs (bio)printing.

2.3. Dual-colour photopolymerization system for (bio)printing

Xolography, different from CAL, uses two different light beams to solid target photoresin (**figure 2(D)**). Specifically, xolography projects intersecting light beams of different wavelengths to photoswitchable photoresin to solidify localized regions. In detail, the blue light generated by a 375-nm laser, as first wavelength, was used to excite a thin layer of photoinitiator molecule from its initial dormant state to a potential state with a finite lifetime. Then the orthogonally placed DLP (3840×2160 pixels ultra-high definition) projected sliced images onto the plane of potential state of photoinitiator molecules to fabricate target model. The method of activating the first wavelength

1
2
3
4 and initiating or inhibiting the polymerization at the second wavelength is called dual-colour
5 photopolymerization (DCP) [45]. Xolography has a printing resolution about ten times higher than
6 CAL without a feedback optimization and shows a volume generation rate about 4-5 orders of
7 magnitude higher than two-photon photopolymerization [42].
8
9

11 **2.4. Comparison of VBP and other bioprinting techniques.**

12
13 3D bioprinting can be divided into three types: the extrusion-based bioprinting, the inkjet-based
14 bioprinting, and the vat photopolymerization-based bioprinting. VBP is one of vat
15 photopolymerization, which is different from the traditional layer-by-layer printing technology as
16 it could create the whole 3D object at once. VBP is inspired by medical CT imaging algorithm,
17 which offers several advantages such as super-fast printing speed (in tens of seconds), contactless
18 printing mode and high cell survival rate (>95%)[68],[77]. The strengths and limitations of VBP
19 in comparison to other bioprinting techniques are shown in Table 3. The contactless, supportless
20 printing modality under visible light and room temperature conditions allowing for more
21 bioprinting scenario than layer-by-layer bioprinting techniques. Meanwhile, the limitations of
22 VBP are included: (i) VBP can only print 3D objects at centimeter-scales (normally less than 10
23 cm). Increasing the size of printing vial as well as the light intensity and light penetration depths
24 might be one of the solutions. Recently, Christophe Moser group proposed a method called
25 volumetric helical additive manufacturing to print structures up to 3 cm × 3 cm × 5 cm [90],[91].
26 (ii) Printing resolution is an important indicator in 3DP, creating high-resolution features remains
27 a challenge for VBP. (iii) multi-material and multi-cellular VBP might be another challenge. (iv)
28 Lack of VBP based (bio)inks. The ideal VBP based (bio)inks should have suitable light penetration
29 depth and excellent biocompatibility.
30
31
32
33
34
35
36
37
38
39
40
41
42
43
44
45

46 **3. Photoresins for VBP**

47 **3.1. Photoinitiators and photocrosslinking reactions**

48
49 Photoinitiator is a key component for a photopolymerization-based biofabrication modality [46].
50
51 Generally, a high concentration of photoinitiator would increase the speed of photopolymerization,
52 while might increase the cytotoxicity as well. The commonly used photoinitiators for
53
54
55
56
57
58
59
60

1
2
3
4 photopolymerization are classified as Type I and Type II (**figure 8(A)**) [47],[48]. Type I
5 photoinitiators are monomolecular, which are the most efficient and commonly used systems in
6 photopolymerization. However, most type I photoinitiators are only reactive under UV light, which
7 is harmful to cells. The typical I of photoinitiators for biomedical applications includes lithium
8 phenyl-2,4,6-trimethylbenzoylphosphinate (LAP) and Irgacure 2959 (**figure 8(B)**), both of them
9 can be initiated under 365 nm of wavelength. Type II of photoinitiators are more complex in their
10 initiating reactions than Type I photoinitiators, which rely on the combination of two molecules,
11 like tris-bipyridyl-ruthenium (II) hexahydrate (Ru) and sodium persulfate (SPS) [49]. The first
12 molecule absorbs the photon, which is often called the photoinitiator (PI) or the photosensitizer
13 (PS). The second molecule is often called coinitiator (Co), which gives the initiating radicals (R*)
14 through photoreaction [50],[51].

15
16
17
18
19
20
21
22
23
24
25 Suitable bioinks are needed for bioprinting of high-fidelity and geometrically complex organ
26 structures to match their mechanical stiffness [52]. For example, brain is the utmost excitement of
27 muscle and softest organ of the human body. It is challenging to choose suitable bioinks for
28 bioprinting functional brain model *in vitro* [53].

32 33 **3.2. (Bio)ink recipes of VBP**

34
35 VBP is a new (bio)printing strategy, which lacks suitable (bio)ink. The continuous development
36 of functional (bio)ink would expand the application range of VBP. Bioprinting is to fabricate living
37 constructs for tissue engineering and regenerative medicine, especially in areas such as
38 transplantation and disease modeling [56], [57]. The design of cell compatible bioinks with a high
39 printing performance is a critical step for this perspective. Currently, gelatin methacryloyl (GelMA)
40 is a commonly used bioink in bioprinting [58]-[61].

41
42
43
44
45
46
47
48
49
50
51
52
53
54
55
56
57
58
59
60
Silkworm silk, a natural protein fiber, has an excellent mechanical property and a good
biocompatibility. Raw silks mainly contain silk sericin (SS) and silk fibroin (SF) [63]-[67].
Recently, Our group extracted both SS and SF from silkworm (*Bombyx mori*) cocoons and mixed
with visible-light photoinitiator combination Ru/SPS to prepare SS and SF (bio)inks (**figure 6 (Ai)**)
[68]. For both SS and SF (bio)inks, a variety of complex constructs were volumetrically

(bio)printed (**figure 6 (A, ii)** and **figure 6 (A, iii)**). Interestingly, SS constructs showed a repeated shrinkage and expansion property. And SF constructs with a double-crosslinked network showed tunable mechanical properties (**figure 6 (A, iv)**). The pristine silk-based (bio)inks expand bioinks library of VBP.

Figure 6 (B) shows another type of photoclick bioink for fast VBP. First, gelatin-norbornene (Gel-NB) was mixed with a multifunctional crosslinker 4-arm-PEG-thiol (PEG4SH). Then 0.05% w/v of LAP was added into the mixture, and UV irradiation was used to crosslink the target structure. PEG4SH was used as a crosslinker to obtain a higher storage modulus than PEG2SH or 3,6-dioxa-1,8-octanedithiol (DODT). The carbic anhydride (CA) was used to synthesize Gel-NB, which was cheaper than GelMA. Optorheological studies was performed using 0.05% w/v of LAP, which showed a better cellular compatibility compared with previous reported I2959 [79].

CAL could use engineered polymer resins (such as acrylic polymers and acrylonitrile butadiene styrene (ABS) polymers) with high viscosities [39]. First, two acrylate polymers bisphenol A glycerolate (1 glycerol/phenol) diacrylate (BPAGDA)/poly (ethylene glycol) diacrylate (PEGDA) (average $M_n = 250$ g/mol) were mixed at a ratio of 3:1 or 7:1 to form acrylate photopolymers (**figure 6 (C)**). Then two photoinitiating system consisted of 5.2 mM photoinitiator camphorquinone (CQ) and 5.2 mM coinitiator ethyl 4-dimethylaminobenzoate (EDAB) was added to form engineered polymer. This mixture was measured to have a considerably high viscosity of $93,000 \pm 5,000$ mPa s (7:1 of BPAGDA/PEGDA formulations). The high viscosity indicated that the relative displacement of the print can be reduced during the printing process, which improved the printing fidelity and the printing resolution. The resin was cured by irradiation with 405 nm light source, and the printed structures were stained for easy optical observation (**figure 6 (C, i)-(C, v)**).

Dual-colour photoinitiator (DCPI) is a photoswitch-incorporated photoinitiating system that requires two different light beams to activate [54]. The first step was irradiated with 375 nm of UV light; thus, the irradiated part was widely absorbed at 450-700 nm, and then the (bio)ink was polymerized under 585 nm of red light. The synthesis of DCPI was divided into three steps (**figure**

1
2
3
4 **6(D)**): first, the syntheses of 5-Cyano-1,2,3,3-tetramethylindolenium iodide and 4-Fluoro-3'-
5 formyl-4'-hydroxybenzophenone; then 5-Cyano-1,2,3,3-tetramethylindolenium iodide and
6 piperidine were dissolved in ethanol; finally, 4-Fluoro-3'-formyl-4'-hydroxybenzophenone was
7 added to the mixture from step 2 and heated to 70°C to form DCPI. High resolution (25 μm) was
8 achieved.
9
10
11
12

13 Recently, Moser *et al* group successfully printed ceramic parts using a volumetric printer
14 [89]. The preparation of ink is shown in **Figure 6(E)**. The ink consists of three parts: (i)
15 polysiloxane (SPR 684) was as a preceramic polysiloxane resin; (ii) 1,4-butanediol-diacrylate
16 (BDDA) was as a crosslinker; (iii) diphenyl-(2,4,6-trimethylbenzoyl)-phosphine oxide (TPO) was
17 as a photoinitiator. The crosslinked preceramic was formed by irradiation with 405 nm of blue
18 light source about 1 min. Then, the green body (CAL-printed structure without debinding and
19 sintering) was converted to polymer-derived ceramic (PDC) during pyrolysis at 1000°C for 48 h.
20 Polysiloxane (SPR 684) is a commercially available material that can be pyrolyzed into ceramics
21 at 1000-2000°C [55]. The viscosity of the ink was 873 mPa s. In short, the process started with a
22 liquid preceramic polymer (PCP), which was solidified into a green body. Then the green body
23 was transformed to a ceramic material, generally referred to as PDC.
24
25
26
27
28
29
30
31
32
33
34

35 **Table 2** shows the currently reported (bio)inks used in VBP, which are divided into two
36 categories: bioink and functional ink. Then, the following part mainly introduces the applications
37 of VBP based on these (bio)inks.
38
39
40

41 **4. Biomedical applications of VBP-based technology**

42 **4.1. Bioprinting**

43 Levato *et al* group used cell-friendly hydrogel bioink to bioprint large living tissue constructs
44 (**figure 7 (A)**) [75]. Except for using a volumetric printer to print human auricle model (**figure 7**
45 (**Aiii**)), they also volumetrically bioprinted meniscal, trabecular, trabecular bone-like constructs,
46 which showed high cell viabilities (>85%) after culturing for 7 d [75]. Levato *et al* group
47 investigated a new method to explore the optical properties of cell-laden hydrogels for VBP and
48 unraveled the culture of organoid structures and the influence of cell on printing resolution [77].
49
50
51
52
53
54
55
56
57
58
59
60

1
2
3
4 In terms of cell culture, researchers used tens of millions of cells to bioprint. They set up a dynamic
5 culture system to culture cells isolated from human liver biopsies (**figure 7 (B)**). Essentially, these
6 organoids were epithelial, which was a cyst-like structure with an inner hollow lumen surrounded
7 by a thin cell (mono)layer [77]. These cell-laden structures were volumetrically bioprinted within
8 20 s and the printed organoids were used as biofactories in established sterile perfusion chambers,
9 opening a new possibility for the future development of self-sustaining biofactories.
10
11

12
13
14
15 Zenobi-Wong *et al* group volumetrically bioprinted a cell-laden branch model of mesoscale
16 vessel lumen size (**figure 7 (C, i)**) [79]. In this study, encapsulated mouse myoblasts muscle cells
17 (C2C12) were used to proliferate, spread, and differentiate into multinucleated contractile
18 myotubes in a soft crosslinked matrix (**figure 7 (C, ii)**), which showed a distinguished cell viability
19 (>95%) upon printing and >90% after 7 d of culture; meanwhile, the differentiation of myotubes
20 was observed after 3 weeks of culture (myosin heavy chain: red, nuclei: blue, scale bars: 200 μm)
21 (**figure 7 (C, iii)**) [79]. The study showed that VBP had the ability to generate complex tissue
22 models such as skeletal muscle with a high-throughput potential.
23
24
25
26
27
28
29
30

31 In our recent study, our group showed that both SS and SF (bio)inks could be volumetrically
32 bioprinted as low as 2.5% (**figure 7 (D)**) [68]. The cell-laden silk (bio)inks (2.5% and 5% SS, 0.5-
33 mM Ru/5-mM SPS; 2.5-10% SF with a single photocrosslinked network, 0.25-mM Ru/2.5-mM
34 SPS) showed favorable cytocompatibility. Specifically, both 2.5% SS and 2.5% SF constructs
35 supported better proliferation rates and viability than constructs with higher silk concentrations.
36 The cytocompatibility of SS and SF bioinks at low-concentrations (2.5%-5%) made them suitable
37 for VBP applications where living cells are encapsulated. Of note, unlike SF.
38
39
40
41
42
43
44

45 Xiao-Hua Qin *et al* group volumetrically bioprinted a centimeter-scale heterocellular bone
46 model contained human mesenchymal stem cells (hMSCs) and co-cultured with human umbilical
47 vein endothelial cell (HUVECs); and the 3D osteocyte was successful differentiated after 42 d of
48 culture [80]. In detail, first, a bioink (5% GelMA, 0.05% LAP, hMSCs) was prepared to bioprint
49 a pre-vascularized bone construct (**figure 8 (A, i)** and (**A, ii**)). After culturing 7 d, the HUVECs
50 cell suspension was injected into a hollow channel (**figure 8 (A, iii)**). **Figure 8 (B)** showed that
51
52
53
54
55
56
57
58
59
60

1
2
3
4 the confocal 3D image after co-culture of 7 d, the red color shows the self-organized endothelial
5 monolayer in lining of channels. Meaningfully, after 3D co-culture of 42 d, the osteoblastic
6 markers (collagen-I, ALP, osteocalcin) and osteocytic markers (Podoplanin, PDPN; dentin matrix
7 acidic phosphoprotein 1, Dmp1) were expression.
8
9
10

11 Cell concentration would affect resolution of VBP. Thus, it is necessary to explore how to
12 bioprint high-fidelity tissue structures in a high concentration or turbid bioinks. Christophe Moser
13 *et al* group used scattering corrected VBP method to manufacture cell-laden complex geometry
14 constructs [96]. As a proof-of-concept, the vasculatures with four hollow channels (the bioink
15 contained 4×10^6 mL⁻¹ of human embryonic kidney 293 cells), which was challenging, were
16 successfully volumetrically bioprinted (**figure 8 C**), expanding the potential of biomedical
17 applications of VBP.
18
19
20
21
22
23
24

25 **4.2. VBP of multi-material and multi-cell**

26 VBP of multiple-material and multiple-cell is important, challenging as well, for heterogeneous
27 tissue-like structures, and some laboratories have made some progresses [81]-[83].
28
29
30

31 By cooperating with other 3DP technologies, VBP has brought some exciting results in
32 heterogeneous tissue-like structures, such as multicellular blood vessel model and localized high-
33 density cell bioprinting [78,84]. Recently, Riccardo Levato *et al* group converged VBP with melt
34 electrowriting (MEW) technology to bioprint intricate, multi-material and mechanical stability
35 tubular structures [84]. Interestingly, inter or outer of MEW mesh (**figure 8 (D)**) and micron-scale
36 fenestrations such as permeable vessels in human body (**figure 8 (E)**) could be volumetrically
37 (bio)printed [85], [86]. In detail, the bioprinting process was divided into four steps: (i) MEW
38 mesh architectures with different pore shapes (*i.e.*, 34° or 70° winding angles) and thicknesses (*i.e.*,
39 20, 30, 40, 60 printed layers) were fabricated; (ii) the MEW mesh was put into the first bioink
40 container (5% w/v GelMA + 0.1% w/v LAP and 1×10^7 cells mL⁻¹ hbMSCs (Human bone marrow-
41 derived mesenchymal stromal cells)) to volumetrically bioprinted first layer (1050 um) hollow
42 tube (outer of MEW mesh) (**figure 8(F)**); (iii) the sample and re-infused the bioink (5% w/v
43 GelMA + 0.1% w/v LAP and 5×10^5 cells mL⁻¹ hbMSCs) was washed and volumetrically
44
45
46
47
48
49
50
51
52
53
54
55
56
57
58
59
60

1
2
3
4 bioprinted second layer (800 μm) around first layer (**figure 8 (G)**); (iv) the sample was washed
5 and cultured overnight, then 1×10^7 cells mL^{-1} GFP-HUVECs (Green fluorescent human umbilical
6 vein endothelial cells) suspension were seeded inner of MEW mesh on the next day, which were
7 rotated 90° every 20 min to create the third layer (80 μm). At last, the researchers merged these
8 two technologies to build a tri-layered cell-laden vessels (**figure 8 (H)**), which expended the
9 potential applications of VBP in vascular tissue engineering.
10
11
12
13
14

15
16 Riccardo Levato et al group converged VBP with extrusion bioprinting technology to print
17 physiologically-relevant models [78]. The characteristic of this hybrid printing technology was
18 permissive high cell densities ($>10^7$ mL^{-1}) printing in a pre-defined spatial location. Specifically,
19 a geometry was printed in a vial filled with bioink using extrusion printer, then this vial was put
20 into a VBP printer to print another intricate geometry with different bioinks (**figure 8 (I)**). Some
21 complex co-culture models like branch vasculature, Einstein's head and pancreatic models were
22 printed (**figure 8 (J)**). The printing time was less 5 min [75,76].
23
24
25
26
27
28

29 **4.3. VBP of personalized tablets**

30
31 3DP technology is applicable for pharmaceutical industry, because of its personalized and highly
32 customized manufacturing ability [69]. 3DP technology could be applied to patient-friendly drug
33 development by adjusting drug dose, shape, flavor, and mining release patterns to meet the
34 individual need, showing a great potential in the pharmaceutical industry [70].
35
36
37
38

39 Goyanes *et al* group successfully prepared printlets (pills) containing paracetamol within 7-
40 17 s using a volumetric printer, for the first time [71]. It is the fastest way to produce personalized
41 oral pills so far. The printing system could divide a light source into three propagation paths and
42 spread it into the resin container bottle to cure the pill in 10 s (**figure 9 (A) and figure 9 (B)**). The
43 images of six pills: PW90-10, PW65-35, PW35-65, PP90-10, PP65-35, PP35-65 were shown in
44 **Figure 9 (C)**. Then the X-ray micro-CT images of different pills (**figure 9 (D)**) and environmental
45 scanning electron microscope (ESEM) images of cross sections of different pills after all
46 processing steps were observed (**figure 9 (E)**). VBP offers a fast way of pharmaceutical
47 development and drug testing, showing unique advantage in personalized medication [72]-[74].
48
49
50
51
52
53
54
55
56
57
58
59
60

4.4. VBP of glass

The traditional glass manufacturing process requires complex procedures with a high temperature melting and a casting process, facing great challenges in manufacturing equipment that can arbitrarily produce complex glass [84], [87]. Next, we introduce the application of VBP in manufacturing both silica glass and silicon oxycarbide ceramics.

Taylor *et al* group designed a microscale computed axial lithography (micro-CAL) system [88], which was capable of printing minimum feature sizes of 20 μm for polymer, and minimum feature sizes of 50 μm for fused silica glass. The green body (**figure 10 (A, i)**) was obtained by curing the silica glass nanocomposite resin. Then the green body was subjected to thermal treatment of debinding steps (**figure 10 (A, ii)**) and then was sintered to obtain a fully dense silica part (**figure 10 (A, iii)**). The prints had unprecedented geometric freedom, low surface roughness, high breaking strength, and optical transparency in fused silica.

Moser *et al* group volumetrically printed silicon oxycarbide ceramics successfully [89]. The printing procedure was divided into two steps (**figure 10 (B)**). First, the 2D images of the printed object was projected at different angles onto the photosensitive polysiloxane preceramic resin (the resin used had a viscosity of 873 mPa s) and cured in the container. Then a ceramic was formed by pyrolysis at 1000°C. The ceramic parts showed resistance in a high temperature for 20 s (**figure 10 (B, i)**), and in HCl and KOH solutions for 1 h (**figure 10 (B, ii)**). **Figure 10 (C)** showed the different types of volumetrically printed glass constructs. Compared with traditional printing and pyrolysis, volumetric printing greatly improves fabrication efficiency and speeds up the model optimization cycle as well.

5. Outlook and future perspectives

In recent years, VBP has gained increasing attention due to its extremely fast printing speed, high cell viability (**Table 4**) and supportless printing modality (**Table 3**). Researchers are focusing on improving printing resolution and fidelity of VBP through hardware and software aspects [41],[96]. Others are exploring and developing novel bioinks for VBP to expand its biomedical applications [100].

1
2
3
4 In future work, to meet complicated biomedical applications such as tissue engineering,
5 regenerative medicine, *et al*, single material can't satisfy these specific functions [92]. Therefore,
6 multi-material and multi-cell VBP is in urgent need [93], [94]. The manufacture of organoids and
7 large-scale tissue structures are hot topic applications [77],[90]. Additionally, *in situ* VBP might
8 be an interesting direction [95].
9
10
11
12

13 Further, artificial intelligence (AI) assisted (bio)printing is a prospect direction. AI (especially
14 machine learning) technique could be used to optimize printing parameters to compensate the cell-
15 induced scattering effects, or to identify the optimized formulations of (bio)resins to improve
16 printing resolution [97]-[100]. Shaochen Chen et al group used machine learning to automatically
17 generate the printer parameters to compensate scattering effects, which significantly improved the
18 printing resolution [101],[102]. At last, it is predictable that VBP could facilitate fast medical
19 device manufacturing such as microneedles, tooth, organ chips and flexible electronics [103],[104].
20
21
22
23
24
25
26
27
28

29 **Acknowledgments**

30 This work was supported by the Guangdong provincial basic and applied basic research fund
31 provincial enterprise joint fund [grant No. 2021A1515220174]. The authors have no other relevant
32 affiliations or financial involvement with any organization or entity with a financial interest in or
33 financial conflict with the subject matter or materials discussed in the manuscript apart from those
34 disclosed.
35
36
37
38
39
40
41
42

43 **Conflict of interests**

44 All other authors declare they have no competing interests.
45
46
47

48 **References:**

- 49 [1] Guillemot F, Mironov V and Nakamura M 2010 Bioprinting is coming of age: report from
50 the International Conference on Bioprinting and Biofabrication in Bordeaux (3B'09)
51 Biofabrication 2 010201
52
53 [2] Groll J, Boland T, Blunk T, Burdick J A, Cho D W, Dalton P D, Derby B, Forgacs G, Li Q,
54 Mironov V A, Moroni L, Nakamura M, Shu W, Takeuchi S, Vozzi G, Woodfield T B F, Xu T,
55
56
57
58
59
60

- 1
2
3 Yoo J J and Malda J 2016 Biofabrication: reappraising the definition of an evolving field
4 Biofabrication 8 013001
5
6 [3] Li G, Wang J, Xu M, Zhang H, Tu C, Yang J, Chen X, Yao Q, Lan P and Xie M 2020
7 Engineered exosome for NIR-triggered drug delivery and superior synergistic chemo-
8 phototherapy in a glioma model Applied Materials Today 20 100723
9
10 [4] Quan H, Zhang T, Xu H, Luo S, Nie J and Zhu X 2020 Photo-curing 3D printing technique
11 and its challenges Bioactive Materials 5 110–5
12
13 [5] Mazumder J 2015 Design for Metallic Additive Manufacturing Machine with Capability for
14 “Certify as You Build” Procedia CIRP 36 187–92
15
16 [6] Suntornnond R, Ng W L, Huang X, Yeow C H E and Yeong W Y 2022 Improving printability
17 of hydrogel-based bio-inks for thermal inkjet bioprinting applications via saponification and heat
18 treatment processes J. Mater. Chem. B 10 5989–6000
19
20 [7] Li X, Liu B, Pei B, Chen J, Zhou D, Peng J, Zhang X, Jia W and Xu T 2020 Inkjet Bioprinting
21 of Biomaterials Chem. Rev. 120 10793–833
22
23 [8] Ng W L, Huang X, Shkolnikov V, Goh G L, Suntornnond R and Yeong W Y 2021 Controlling
24 Droplet Impact Velocity and Droplet Volume: Key Factors to Achieving High Cell Viability in
25 Sub-Nanoliter Droplet-based Bioprinting Int J Bioprint 8 424
26
27 [9] Xu T, Zhao W, Zhu J-M, Albanna M Z, Yoo J J and Atala A 2013 Complex heterogeneous
28 tissue constructs containing multiple cell types prepared by inkjet printing technology Biomaterials
29 34 130–9
30
31 [10] Ong C S, Fukunishi T, Zhang H, Huang C Y, Nashed A, Blazeski A, DiSilvestre D, Vricella
32 L, Conte J, Tung L, Tomaselli G F and Hibino N 2017 Biomaterial-Free Three-Dimensional
33 Bioprinting of Cardiac Tissue using Human Induced Pluripotent Stem Cell Derived
34 Cardiomyocytes Sci Rep 7 4566
35
36 [11] Fu Z, Naghieh S, Xu C, Wang C, Sun W and Chen X 2021 Printability in extrusion
37 bioprinting Biofabrication 13 033001
38
39 [12] Zhang Y S, Haghighiastiani G, Hübscher T, Kelly D J, Lee J M, Lutolf M, McAlpine M C,
40 Yeong W Y, Zenobi-Wong M and Malda J 2021 3D extrusion bioprinting Nat Rev Methods
41 Primers 1 75
42
43 [13] Ravanbakhsh H, Karamzadeh V, Bao G, Mongeau L, Juncker D and Zhang Y S 2021
44 Emerging Technologies in Multi-Material Bioprinting Advanced Materials 33 2104730
45
46 [14] Tavafoghi M, Darabi M A, Mahmoodi M, Tutar R, Xu C, Mirjafari A, Billi F, Swieszkowski
47 W, Nasrollahi F, Ahadian S, Hosseini V, Khademhosseini A and Ashammakhi N 2021
48 Multimaterial bioprinting and combination of processing techniques towards the fabrication of
49 biomimetic tissues and organs Biofabrication 13 042002
50
51 [15] Ying G, Manríquez J, Wu D, Zhang J, Jiang N, Maharjan S, Hernández Medina D H and
52 Zhang Y S 2020 An open-source handheld extruder loaded with pore-forming bioink for in situ
53 wound dressing Materials Today Bio 8 100074
54
55 [16] Cheng R Y, Eylert G, Garipey J-M, He S, Ahmad H, Gao Y, Priore S, Hakimi N, Jeschke M
56 G and Günther A 2020 Handheld instrument for wound-conformal delivery of skin precursor
57 sheets improves healing in full-thickness burns Biofabrication 12 025002
58
59
60

- 1
2
3 [17] Duan B, Hockaday L A, Kang K H and Butcher J T 2013 3D Bioprinting of heterogeneous
4 aortic valve conduits with alginate/gelatin hydrogels *J. Biomed. Mater. Res.* 101A 1255–64
- 5 [18] Chen M Y, Skewes J, Woodruff M A, Dasgupta P and Rukin N J 2020 Multi-colour extrusion
6 fused deposition modelling: a low-cost 3D printing method for anatomical prostate cancer models
7 *Scientific Reports* 10 10004
- 8
9 [19] Onoe H, Okitsu T, Itou A, Kato-Negishi M, Gojo R, Kiriya D, Sato K, Miura S, Iwanaga S,
10 Kuribayashi-Shigetomi K, Matsunaga Y T, Shimoyama Y and Takeuchi S 2013 Metre-long cell-
11 laden microfibres exhibit tissue morphologies and functions *Nature Mater* 12 584–590
- 12 [20] de Beer M P, van der Laan H L, Cole M A, Whelan R J, Burns M A and Scott T F 2019
13 Rapid, continuous additive manufacturing by volumetric polymerization inhibition patterning. *Sci*
14 *Adv* 5 eaau8723
- 15 [21] Lee M, Rizzo R, Surman F and Zenobi-Wong M 2020 Guiding Lights: Tissue Bioprinting
16 Using Photoactivated Materials *Chem. Rev.* 120 10950–1027
- 17 [22] Levato R, Dudaryeva O, Garciamendez-Mijares C E, Kirkpatrick B E, Rizzo R, Schimelman
18 J, Anseth K S, Chen S, Zenobi-Wong M and Zhang Y S 2023 Light-based vat-polymerization
19 bioprinting *Nat Rev Methods Primers* 3 47
- 20 [23] Ng W L, Lee J M, Zhou M, Chen Y-W, Lee K-X A, Yeong W Y and Shen Y-F 2020 Vat
21 polymerization-based bioprinting—process, materials, applications and regulatory challenges
22 *Biofabrication* 12 022001
- 23 [24] Daly A C, Prendergast M E, Hughes A J and Burdick J A 2021 Bioprinting for the Biologist
24 *Cell* 184 18–32
- 25 [25] Levato R, Lim K S, Li W, Asua A U, Peña L B, Wang M, Falandt M, Bernal P N, Gawlitta
26 D, Zhang Y S, Woodfield T B F and Malda J 2021 High-resolution lithographic biofabrication of
27 hydrogels with complex microchannels from low-temperature-soluble gelatin bioresins *Materials*
28 *Today Bio* 12 100162
- 29 [26] Cheng J, Wang R, Sun Z, Liu Q, He X, Li H, Ye H, Yang X, Wei X, Li Z, Jian B, Deng W
30 and Ge Q 2022 Centrifugal multimaterial 3D printing of multifunctional heterogeneous objects
31 *Nat Commun* 13 7931
- 32 [27] Tumbleston J R, Shirvanyants D, Ermoshkin N, Januszewicz R, Johnson A R, Kelly D, Chen
33 K, Pinschmidt R, Rolland J P, Ermoshkin A, Samulski E T and DeSimone J M 2015 Additive
34 manufacturing. Continuous liquid interface production of 3D objects. *Science* 347 1349–52
- 35 [28] Lipkowitz G, Samuelsen T, Hsiao K, Lee B, Dulay M T, Coates I, Lin H, Pan W, Toth G,
36 Tate L, Shaqfeh E S G and DeSimone J M 2022 Injection continuous liquid interface production
37 of 3D objects. *Sci Adv* 8 eabq3917 3D Bioprinting: from Benches to Translational Applications.
- 38 [29] Kelly B E, Bhattacharya I, Shusteff M, Panas R M, Taylor H K and Spadaccini C M 2017
39 Computed Axial Lithography (CAL): Toward Single Step 3D Printing of Arbitrary Geometries 11
- 40 [30] Cano-Vicent A, Tambuwala M M, Hassan Sk S, Barh D, Aljabali A A A, Birkett M, Arjunan
41 A and Serrano-Aroca Á 2021 Fused deposition modelling: Current status, methodology,
42 applications and future prospects *Additive Manufacturing* 47 102378
- 43
44
45
46
47
48
49
50
51
52
53
54
55
56
57
58
59
60

- 1
2
3 [31] Murphy C A, Lim K S and Woodfield T B F 2022 Next Evolution in Organ-Scale
4 Biofabrication: Bioresin Design for Rapid High-Resolution Vat Polymerization *Advanced*
5 *Materials* 34 2107759
6
7 [32] Gu Z, Fu J, Lin H and He Y 2020 Development of 3D bioprinting: From printing methods
8 to biomedical applications *Asian Journal of Pharmaceutical Sciences* 15 529–57
9
10 [33] Moroni L, Boland T, Burdick J A, De Maria C, Derby B, Forgacs G, Groll J, Li Q, Malda J,
11 Mironov V A, Mota C, Nakamura M, Shu W, Takeuchi S, Woodfield T B F, Xu T, Yoo J J and
12 Vozzi G 2018 *Biofabrication: A Guide to Technology and Terminology. Trends Biotechnol* 36
13 384–402
14
15 [34] de Ruijter M, Ribeiro A, Dokter I, Castilho M and Malda J 2019 Simultaneous
16 Micropatterning of Fibrous Meshes and Bioinks for the Fabrication of Living Tissue Constructs.
17 *Adv Healthc Mater* 8 e1800418
18
19 [35] Bordini E A F, Cassiano F B, Bronze-Uhle E S, Alamo L, Hebling J, de Souza Costa C A
20 and Soares D G 2022 Chitosan in association with osteogenic factors as a cell-homing platform
21 for dentin regeneration: Analysis in a pulp-in-a-chip model. *Dent Mater* 38 655–69
22
23 [36] Billiet T, Vandenhoute M, Schelfhout J, Van Vlierberghe S and Dubrue P 2012 A review of
24 trends and limitations in hydrogel-rapid prototyping for tissue engineering *Biomaterials* 33 6020–
25 41
26
27 [37] Gudapati H, Dey M and Ozbolat I 2016 A comprehensive review on droplet-based
28 bioprinting: Past, present and future *Biomaterials* 102 20–42
29
30 [38] Shusteff M, Browar A E M, Kelly B E, Henriksson J, Weisgraber T H, Panas R M, Fang N
31 X and Spadaccini C M 2017 One-step volumetric additive manufacturing of complex polymer
32 structures *Sci. Adv.* 3 eaa05496
33
34 [39] Kelly B E, Bhattacharya I, Heidari H, Shusteff M, Spadaccini C M and Taylor H K 2019
35 Volumetric additive manufacturing via tomographic reconstruction *Science* 363 1075–9
36
37 [40] Matlock A, Zhu J and Tian L 2023 Multiple-scattering simulator-trained neural network for
38 intensity diffraction tomography *Opt. Express* 31 4094–107
39
40 [41] Loterie D, Delrot P and Moser C 2020 High-resolution tomographic volumetric additive
41 manufacturing *Nat Commun* 11 852
42
43 [42] Regehly M, Garmshausen Y, Reuter M, König N F, Israel E, Kelly D P, Chou C-Y, Koch K,
44 Asfari B and Hecht S 2020 Xolography for linear volumetric 3D printing *Nature* 588 620–4
45
46 [43] Ehsan A A, Rahim M S and Woei H C 2019 Projection Optics Design for Projection
47 Stereolithography 3D Printer 2019 IEEE Regional Symposium on Micro and Nanoelectronics
48 (RSM) 2019 IEEE Regional Symposium on Micro and Nanoelectronics (RSM) (Pahang, Malaysia:
49 IEEE) pp 160–3
50
51 [44] Orth A, Sampson K L, Zhang Y, Ting K, Webber D, Egmond D A van, Laqua K, Lacelle T,
52 Fatehi D, Boisvert J and Paquet C 2022 Optical Scattering Tomography for Volumetric Additive
53 Manufacturing *Conference on Lasers and Electro-Optics (Optica Publishing Group)* p ATh1D.3
54
55 [45] Swainson W K 1977 Method, medium and apparatus for producing three-dimensional
56 figureure product
57
58
59
60

- 1
2
3 [46] Goodarzi Hosseinabadi H, Dogan E, Miri A K and Ionov L 2022 Digital Light Processing
4 Bioprinting Advances for Microtissue Models ACS Biomater. Sci. Eng. 8 1381–95
5 [47] Ligon S C, Liska R, Stampfl J, Gurr M and Mülhaupt R 2017 Polymers for 3D Printing and
6 Customized Additive Manufacturing Chem. Rev. 117 10212–90
7 [48] Bagheri A and Jin J 2019 Photopolymerization in 3D Printing ACS Appl. Polym. Mater. 1
8 593–611
9 [49] Liu S, Borjigin T, Schmitt M, Morlet-Savary F, Xiao P and Lalevée J 2023 High-
10 Performance Photoinitiating Systems for LED-Induced Photopolymerization Polymers 15
11 [50] Shi S, Croutxé-Barghorn C and Allonas X 2017 Photoinitiating systems for cationic
12 photopolymerization: Ongoing push toward long wavelengths and low light intensities Progress in
13 Polymer Science 65 1–41
14 [51] Ley C, Carre C, Ibrahim A and Allonas X 2017 Application of High Performance
15 Photoinitiating Systems for Holographic Grating Recording. InTech pp 375–404
16 [52] Wang M, Li W, Hao J, Gonzales A 3rd, Zhao Z, Flores R S, Kuang X, Mu X, Ching T, Tang
17 G, Luo Z, Garciamendez-Mijares C E, Sahoo J K, Wells M F, Niu G, Agrawal P, Quiñones-
18 Hinojosa A, Eggan K and Zhang Y S 2022 Molecularly cleavable bioinks facilitate high-
19 performance digital light processing-based bioprinting of functional volumetric soft tissues. Nat
20 Commun 13 3317
21 [53] Axpe E, Orive G, Franze K and Appel E A 2020 Towards brain-tissue-like biomaterials. Nat
22 Commun 11 3423
23 [54] Wang B, Engay E, Stubbe P R, Moghaddam S Z, Thormann E, Almdal K, Islam A and Yang
24 Y 2022 Stiffness control in dual color tomographic volumetric 3D printing Nat Commun 13 367
25 [55] Martinez-Crespiera S, Ionescu E, Kleebe H J and Riedel R 2011 Pressureless synthesis of
26 fully dense and crack-free SiOC bulk ceramics via photo-crosslinking and pyrolysis of a
27 polysiloxane Journal of The European Ceramic Society 31 913–9
28 [56] Lian L, Zhou C, Tang G, Xie M, Wang Z, Luo Z, Japo J, Wang D, Zhou J, Wang M, Li W,
29 Maharjan S, Ruelas M, Guo J, Wu X and Zhang Y S 2022 Uniaxial and Coaxial Vertical Embedded
30 Extrusion Bioprinting Advanced Healthcare Materials 11 2102411
31 [57] Luo Z, Tang G, Ravanbakhsh H, Li W, Wang M, Kuang X, Garciamendez-Mijares C E, Lian
32 L, Yi S, Liao J, Xie M, Guo J, Zhou Z and Zhang Y S 2022 Vertical Extrusion Cryo(bio)printing
33 for Anisotropic Tissue Manufacturing Advanced Materials 34 2108931
34 [58] Anandkrishnan N, Ye H, Guo Z, Chen Z, Mentkowski K I, Lang J K, Rajabian N, Andreadis
35 S T, Ma Z, Spornyak J A, Lovell J F, Wang D, Xia J, Zhou C and Zhao R 2021 Fast
36 Stereolithography Printing of Large-Scale Biocompatible Hydrogel Models Advanced healthcare
37 materials 10
38 [59] Ge Q, Chen Z, Cheng J, Zhang B, Zhang Y F, Li H, He X, Yuan C, Liu J, Magdassi S and
39 Qu S 2021 3D printing of highly stretchable hydrogel with diverse UV curable polymers Sci. Adv.
40 7 eaba4261
41 [60] Li W, Wang M, Mille L S, Robledo Lara J A, Huerta V, Uribe Velázquez T, Cheng F, Li H,
42 Gong J, Ching T, Murphy C A, Lesha A, Hassan S, Woodfield T B F, Lim K S and Zhang Y S
43
44
45
46
47
48
49
50
51
52
53
54
55
56
57
58
59
60

2021 A Smartphone-Enabled Portable Digital Light Processing 3D Printer *Adv Mater* 33 e2102153

[61] Wu D, Yu Y, Tan J, Huang L, Luo B, Lu L and Zhou C 2018 3D bioprinting of gellan gum and poly (ethylene glycol) diacrylate based hydrogels to produce human-scale constructs with high-fidelity *Materials & Design* 160 486–95

[62] Li W, Mille L S, Robledo J A, Uribe T, Huerta V and Zhang Y S 2020 Recent Advances in Formulating and Processing Biomaterial Inks for Vat Polymerization-Based 3D Printing *Adv. Healthcare Mater.* 9 2000156

[63] Kim S H, Hong H, Ajiteru O, Sultan M T, Lee Y J, Lee J S, Lee O J, Lee H, Park H S, Choi K Y, Lee J S, Ju H W, Hong I-S and Park C H 2021 3D bioprinted silk fibroin hydrogels for tissue engineering *Nature protocols* 16 5484-532

[64] De Santis M M, Alsafadi H N, Tas S, Bölükbas D A, Prithiviraj S, Da Silva I A N, Mittendorfer M, Ota C, Stegmayr J, Daoud F, Königshoff M, Swärd K, Wood J A, Tassieri M, Bourguine P E, Lindstedt S, Mohlin S and Wagner D E 2021 Extracellular-Matrix-Reinforced Bioinks for 3D Bioprinting Human Tissue. *Adv Mater* 33 e2005476

[65] Xue B, Zhang Y, Xu M, Wang C, Huang J, Zhang H, Meng S, Xie M, Tao A and Li X 2019 Curcumin-Silk Fibroin Nanoparticles for Enhanced Anti- *Candida albicans* Activity In Vitro and In Vivo *J Biomed Nanotechnol* 15 769–78

[66] Xie M, Li Y, Zhao Z, Chen A, Li J, Li Z, Li G and Lin X 2016 Development of silk fibroin-derived nanofibrous drug delivery system in supercritical CO₂ *Materials Letters* 167 175–8

[67] Chawla S, Midha S, Sharma A and Ghosh S 2018 Silk-Based Bioinks for 3D Bioprinting *Advanced Healthcare Materials* 7 1701204

[68] Xie M, Lian L, Mu X, Luo Z, Garciamendez-Mijares C E, Zhang Z, López A, Manríquez J, Kuang X, Wu J, Sahoo J K, González F Z, Li G, Tang G, Maharjan S, Guo J, Kaplan D L and Zhang Y S 2023 Volumetric additive manufacturing of pristine silk-based (bio)inks *Nat Commun* 14 210

[69] Zhu X, Li H, Huang L, Zhang M, Fan W and Cui L 2020 3D printing promotes the development of drugs *Biomedicine & Pharmacotherapy* 131 110644

[70] Kim J H, Kim K and Jin H-E 2022 Three-Dimensional Printing for Oral Pharmaceutical Dosage Forms *J. Pharm. Investig.* 52 293–317

[71] Rodríguez-Pombo L, Xu X, Seijo-Rabina A, Ong J J, Alvarez-Lorenzo C, Rial C, Nieto D, Gaisford S, Basit A W and Goyanes A 2022 Volumetric 3D printing for rapid production of medicines *Additive Manufacturing* 52 102673

[72] Xu M, Li G, Zhang H, Chen X, Li Y, Yao Q and Xie M 2020 Sequential delivery of dual drugs with nanostructured lipid carriers for improving synergistic tumor treatment effect *Drug Delivery* 27 983–95

[73] Shen Y, Liang L, Zhang S, Huang D, Zhang J, Xu S, Liang C and Xu W 2018 Organelle-targeting surface-enhanced Raman scattering (SERS) nanosensors for subcellular pH sensing *Nanoscale* 10 1622–30

[74] Kong F, Li G, Tang Y, Xi S, Loong J, Li M, Li H, Cheng W, Zhu W, Mo J, Gong Y, Tang H, Zhao Y, Zhang Y, Ma S, Guan X, Ma N, Xie M and Liu M 2021 Targeting tumor lineage

1
2
3 plasticity in hepatocellular carcinoma using an anti-CLDN6 antibody-drug conjugate *Sci. Transl.*
4 *Med.* 13 eabb6282

5
6 [75] Bernal P N, Delrot P, Loterie D, Li Y, Malda J, Moser C and Levato R 2019 Volumetric
7 Bioprinting of Complex Living-Tissue Constructs within Seconds *Adv. Mater.* 31 1904209

8 [76] Lim K S, Levato R, Costa P F, Castilho M D, Alcalá-Orozco C R, Van Dorenmalen K M A,
9 Melchels F P W, Gawlitta D, Hooper G J, Malda J and Woodfield T B F 2018 Bio-resin for high
10 resolution lithography-based biofabrication of complex cell-laden constructs *Biofabrication* 10
11 034101

12
13 [77] P.N. Bernal P N, Bouwmeester M, Madrid-Wolff J, Falandt M, Florczak S, Rodriguez N G,
14 Li Y, Größbacher G, Samsom R-A, van Wolferen M, van der Laan L J W, Delrot P, Loterie D,
15 Malda J, Moser C, Spee B and Levato R 2022 Volumetric Bioprinting of Organoids and Optically
16 Tuned Hydrogels to Build Liver-Like Metabolic Biofactories. *Adv Mater* 34 e2110054

17 [78] Ribezzi D, Gueye M, Florczak S, Dusi F, De Vos D, Manente F, Hierholzer A, Fussenegger
18 M, Caiazzo M, Blunk T, Malda J and Levato R 2023 Shaping Synthetic Multicellular and Complex
19 Multimaterial Tissues via Embedded Extrusion-Volumetric Printing of Microgels *Advanced*
20 *Materials* 2301673

21 [79] R, Ruetsche D, Liu H and Zenobi-Wong M 2021 Optimized Photoclick (Bio)Resins for Fast
22 Volumetric Bioprinting *Advanced Materials* 33 2102900

23 [80] Gehlen J, Qiu W, Schädli G N, Müller R and Qin X-H 2023 Tomographic volumetric
24 bioprinting of heterocellular bone-like tissues in seconds *Acta Biomaterialia* 156 49–60

25 [81] Bertsch P, Diba M, Mooney D J and Leeuwenburgh S C G 2023 Self-Healing Injectable
26 Hydrogels for Tissue Regeneration. *Chem Rev* 123 834–73

27 [82] Ma J and Wu C 2022 Bioactive inorganic particles-based biomaterials for skin tissue
28 engineering *Exploration* 2 20210083

29 [83] Peng Y, Zhuang Y, Liu Y, Le H, Li D, Zhang M, Liu K, Zhang Y, Zuo J and Ding J 2023
30 Bioinspired gradient scaffolds for osteochondral tissue engineering *Exploration* 3 20210043

31 [84] Größbacher G, Bartolf-Kopp M, Gergely C, Bernal P N, Florczak S, de Ruijter M, Rodriguez
32 N G, Groll J, Malda J, Jüngst T and Levato R Volumetric Printing across Melt Electrowritten
33 Scaffolds Fabricates Multi-Material Living Constructs with Tunable Architecture and Mechanics
34 *Advanced Materials* n/a 2300756

35 [85] van Genderen A M, Jansen K, Kristen M, van Duijn J, Li Y, Schuurmans C C L, Malda J,
36 Vermonden T, Jansen J, Masereeuw R and Castilho M 2020 Topographic Guidance in Melt-
37 Electrowritten Tubular Scaffolds Enhances Engineered Kidney Tubule Performance. *Frontiers in*
38 *Bioengineering and Biotechnology* 8 617364

39 [86] Xie C, Gao Q, Wang P, Shao L, Yuan H, Fu J, Chen W and He Y 2019 Structure-induced
40 cell growth by 3D printing of heterogeneous scaffolds with ultrafine fibers *Materials & Design*
41 181 108092

42 [87] Zhang H, Huang L, Tan M, Zhao S, Liu H, Lu Z, Li J and Liang Z 2022 Overview of 3D-
43 Printed Silica Glass Micromachines 13 81

- [88] Toombs J T, Luitz M, Cook C C, Jenne S, Li C C, Rapp B E, Kotz-Helmer F and Taylor H K 2022 Volumetric additive manufacturing of silica glass with microscale computed axial lithography *Science* 376 308-12
- [89] Kollep M, Konstantinou G, Madrid-Wolff J, Boniface A, Hagelüken L, Sasikumar P V W, Blugan G, Delrot P, Loterie D, Brugger J and Moser C 2022 Tomographic Volumetric Additive Manufacturing of Silicon Oxycarbide Ceramics *Adv Eng Mater* 24 2101345
- [90] Boniface A, Maître F, Madrid-Wolff J and Moser C 2023 Volumetric helical additive manufacturing *gxfzz* 4 1
- [91] Vock P, Soucek M, Daepf M and Kalender W A 1990 Lung: spiral volumetric CT with single-breath-hold technique. *Radiology* 176 864–7
- [92] Liu Y, Xie M, Wang S, Zheng Q, Chen A and Deng Q 2013 Facile fabrication of high performances MTX nanocomposites with natural biomembrane bacterial nanoparticles using GP *Materials Letters* 100 248–51
- [93] Warner J, Soman P, Zhu W, Tom M and Chen S 2016 Design and 3D Printing of Hydrogel Scaffolds with Fractal Geometries *ACS Biomater. Sci. Eng.* 2 1763-70
- [94] Ravanbakhsh H, Karamzadeh V, Bao G, Mongeau L, Juncker D and Zhang Y S 2021 Emerging Technologies in Multi-Material Bioprinting *Advanced Materials* 33 2104730
- [95] Hakimi N, Cheng R, Leng L, Sotoudehfar M, Ba P Q, Bakhtyar N, Amini-Nik S, Jeschke M G and Günther A 2018 Handheld skin printer: in situ formation of planar biomaterials and tissues. *Lab Chip* 18 1440–1451
- [96] Madrid-Wolff J, Boniface A, Loterie D, Delrot P and Moser C 2022 Controlling Light in Scattering Materials for Volumetric Additive Manufacturing *Advanced Science* 9 2105144D.
- [97] Orth A, Sampson K L, Ting K, Boisvert J and Paquet C 2021 Correcting ray distortion in tomographic additive manufacturing *Opt. Express* 29 11037
- [98] Bhattacharya I, Toombs J and Taylor H 2021 High fidelity volumetric additive manufacturing *Additive Manufacturing* 47 102299
- [99] Rackson C M, Champley K M, Toombs J T, Fong E J, Bansal V, Taylor H K, Shusteff M and McLeod R R 2021 Object-space optimization of tomographic reconstructions for additive manufacturing *Additive Manufacturing* 48 102367
- [100] Cook C C, Fong E J, Schwartz J J, Porcincula D H, Kaczmarek A C, Oakdale J S, Moran B D, Champley K M, Rackson C M, Muralidharan A, McLeod R R and Shusteff M 2020 Highly Tunable Thiol-Ene Photorecins for Volumetric Additive Manufacturing *Adv. Mater.* 32 2003376
- [101] Guan J, You S, Xiang Y, Schimelman J, Alido J, Ma X, Tang M and Chen S 2022 Compensating the cell-induced light scattering effect in light-based bioprinting using deep learning *Biofabrication* 14 015011
- [102] You S, Guan J, Alido J, Hwang H H, Yu R, Kwe L, Su H and Chen S 2020 Mitigating Scattering Effects in Light-Based Three-Dimensional Printing Using Machine Learning *Journal of Manufacturing Science and Engineering* 142 081002
- [103] Xu M, Liu Y, Yang K, Li S, Wang M, Wang J, Yang D, Shkunov M, Silva S R P, Castro F A and Zhao Y 2023 Minimally invasive power sources for implantable electronics *Exploration* 20220106

1
2
3 [104] Leng F, Zheng M and Xu C 2021 3D-printed microneedles with open groove channels
4 for liquid extraction *Exploration* **1** 20210109
5
6
7
8
9
10
11
12
13
14
15
16
17
18
19
20
21
22
23
24
25
26
27
28
29
30
31
32
33
34
35
36
37
38
39
40
41
42
43
44
45
46
47
48
49
50
51
52
53
54
55
56
57
58
59
60

Accepted Manuscript

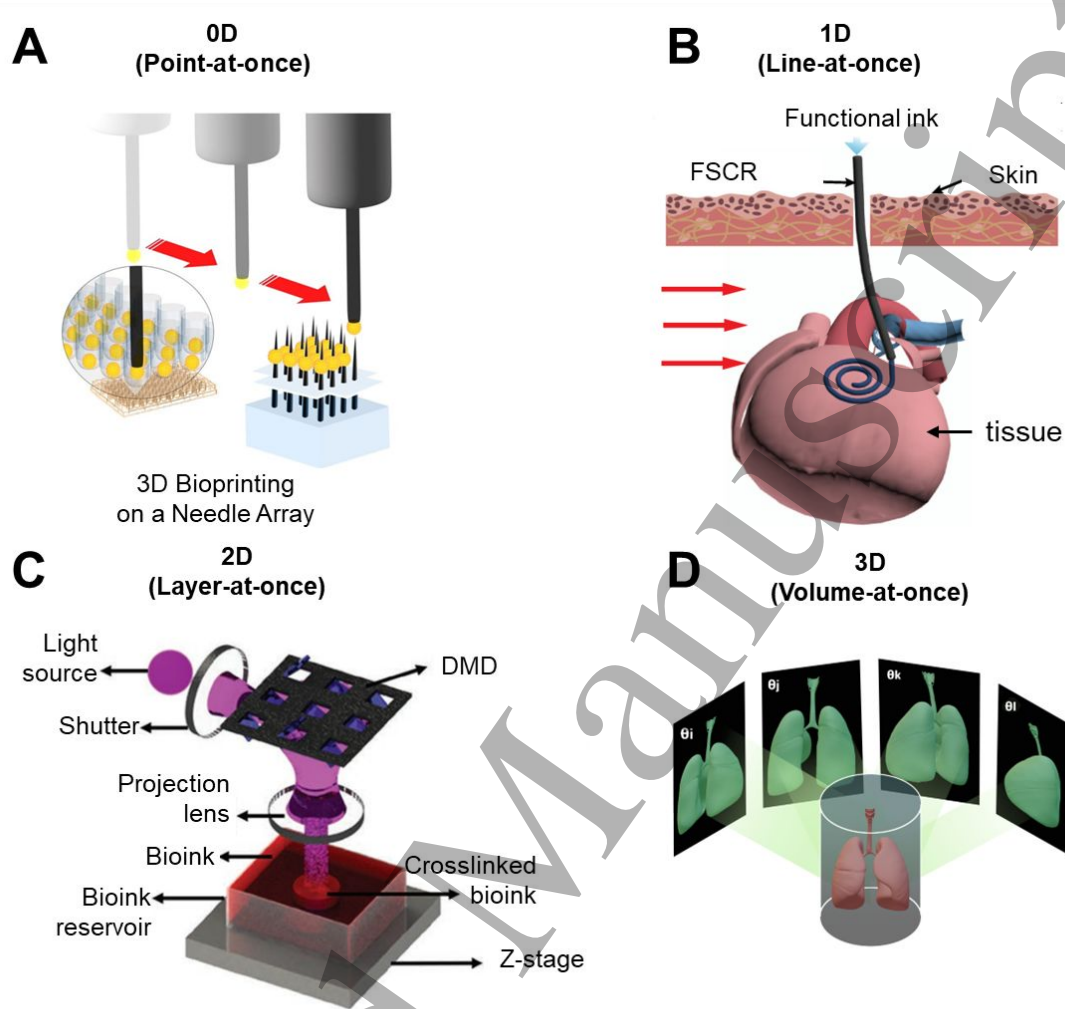


Figure 1. Schematic of 3DP classification in terms of dimensions. **(A)** Schematic of 1D bioprinting, such as inkjet bioprinting. Reproduced with permission [10]. Copyright 2017, Springer Nature Inc. **(B)** Schematic of 1D bioprinting, such as extrusion bioprinting. Reproduced with permission [18]. Copyright 2020, Springer Nature Inc. **(C)** The digital light processing (DLP) printing process, such as DLP. Reproduced with permission [28]. Copyright 2019, John Wiley & Sons Inc. **(D)** Schematic of VBP. Printing all points of entire object simultaneously. Such as CAL. DLP: Digital-light processing. CLIP: Continuous liquid interface printing. iCLIP: Injection continuous liquid interface production. CAL: Computed axial lithography. DMD: Digital micromirror device. VBP: Volumetric bioprinting.

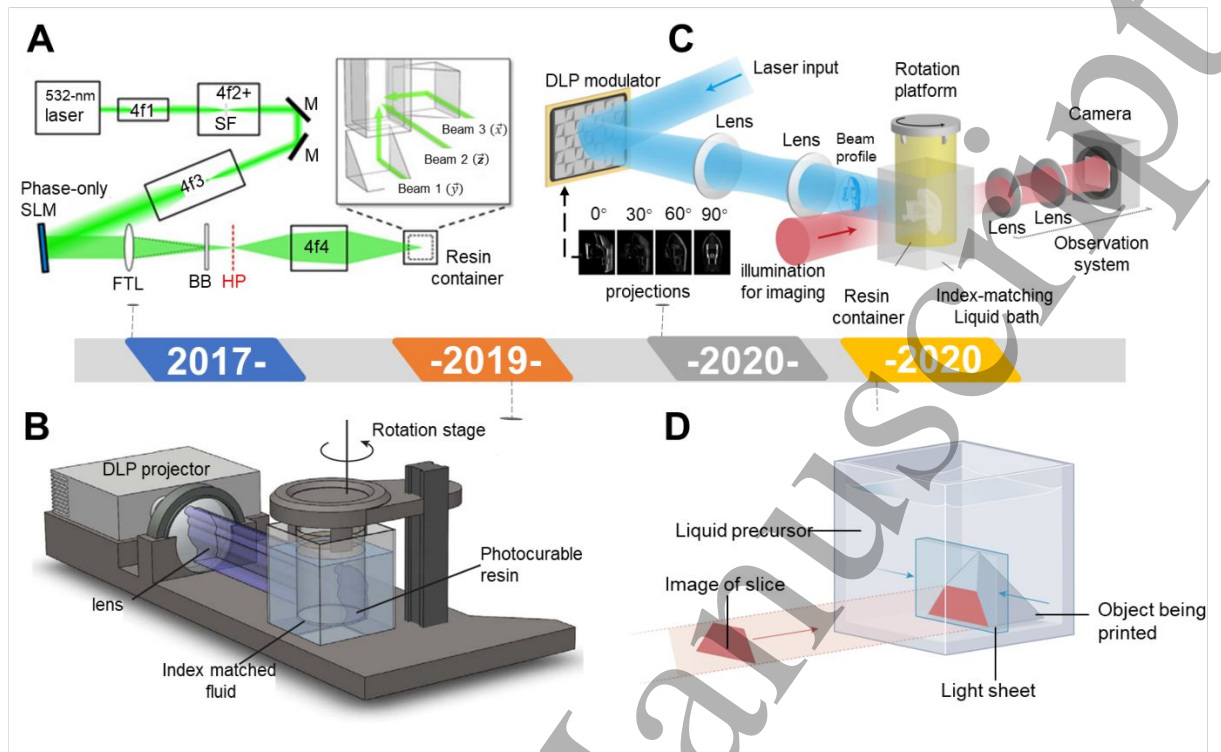


Figure 2. Development of VBP and related bioprinting techniques. **(A)** Schematic of holographic volumetric 3D fabrication system[38]. Reproduced with permission [38]. Copyright 2017, The American Association for the Advancement of Science. **(B)** Schematic of CAL volumetric 3D fabrication system. Reproduced with permission [39]. Copyright 2019, The American Association for the Advancement of Science. **(C)** Schematic of high-resolution tomographic 3D fabrication system. Reproduced with permission [41]. Copyright 2020, Springer Nature Inc. **(D)** Schematic of xolography 3D fabrication system. Reproduced with permission [42]. Copyright 2020, Springer Nature Inc. SLM: Spatial light modulators. FTL: Fourier-transform lens. BB: Beam block. HP: Hologram plane. M: Mirror. DLP: Digital-light processing. CAL: Computed axial lithography. VBP: Volumetric bioprinting.

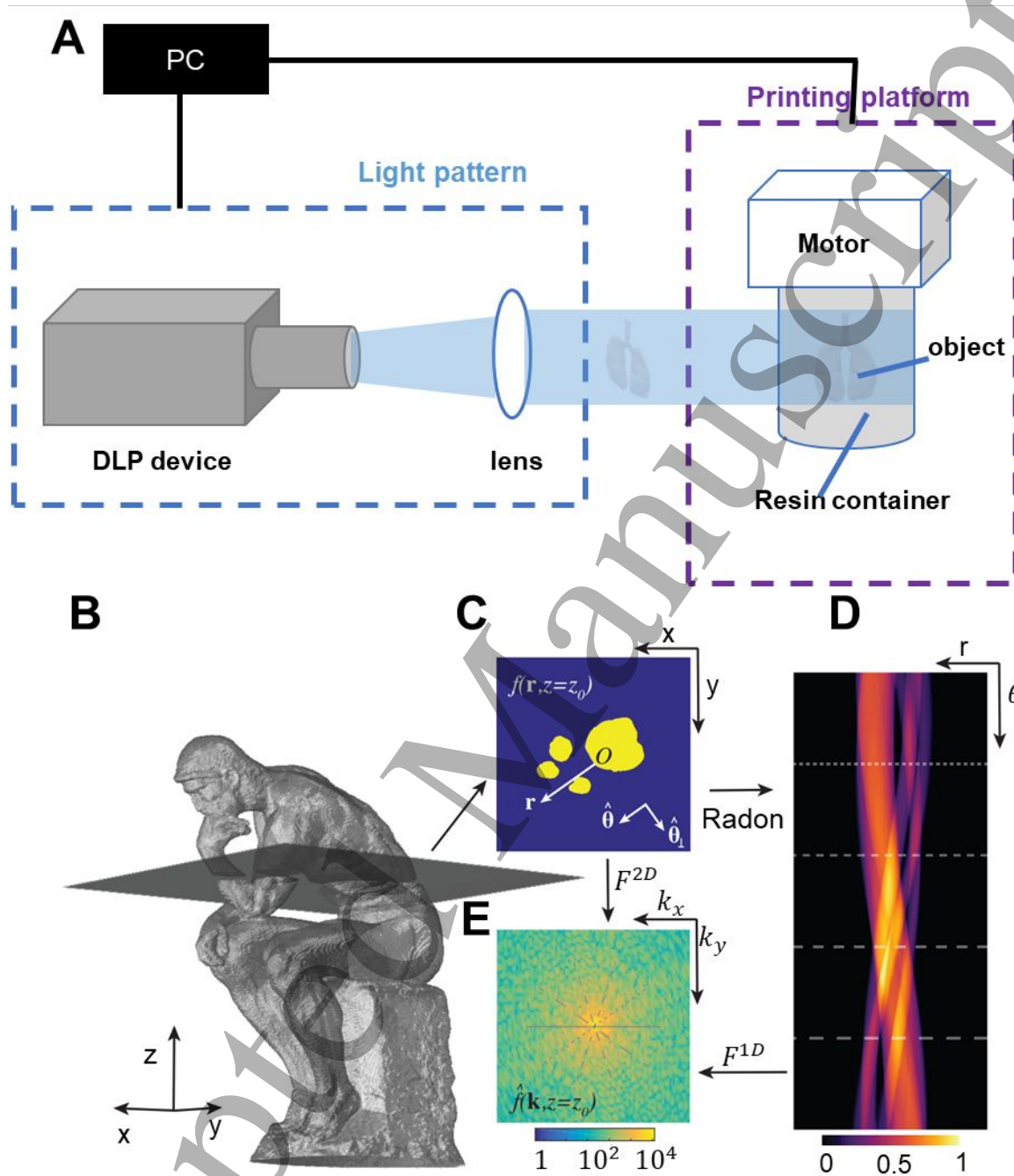


Figure 3. Schematic of DLP based VBP printers and slice analysis of 3D structure. (A) Typical DLP-based setup of VBP system. (B) 3D target object of the “Thinker”. (C) Z cross section from (B). (D) Radon transforms of the “Thinker”. (E) 2D Fourier transform of the Thinker construct. (B-D) Reproduced with permission [39] Copyright 2020, The American Association for the Advancement of Science. PC: Personal computer. DMD: Digital micromirror device. DLP: Digital-light processing. VBP: Volumetric bioprinting.

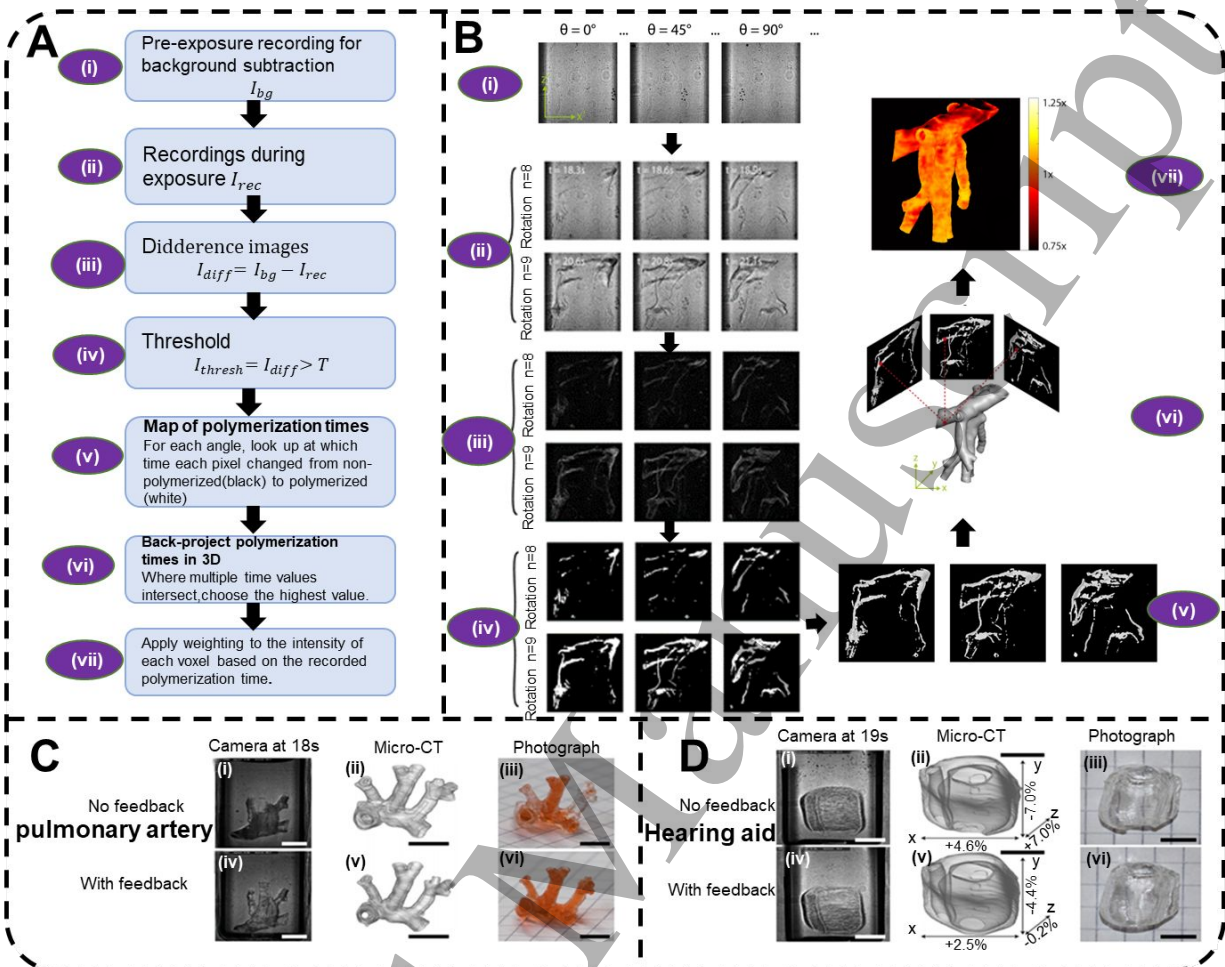
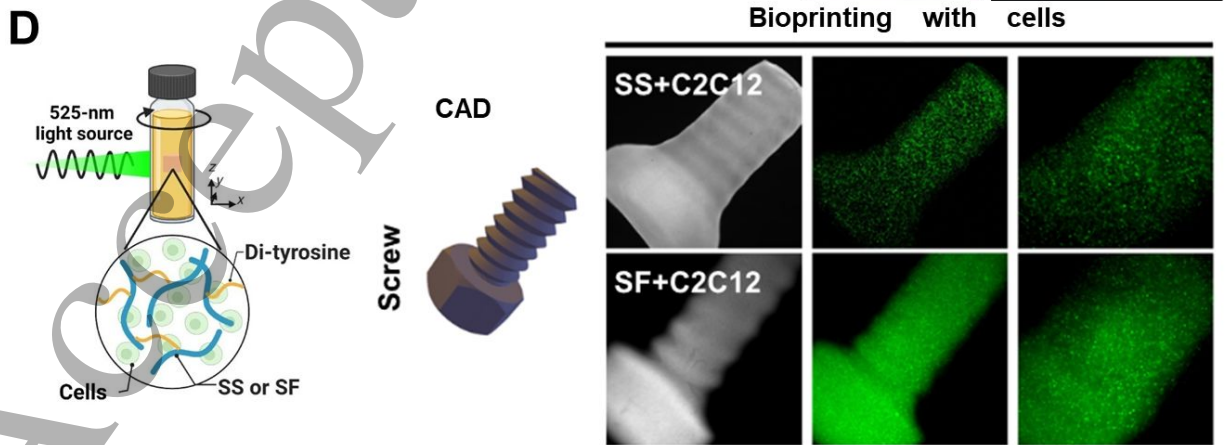
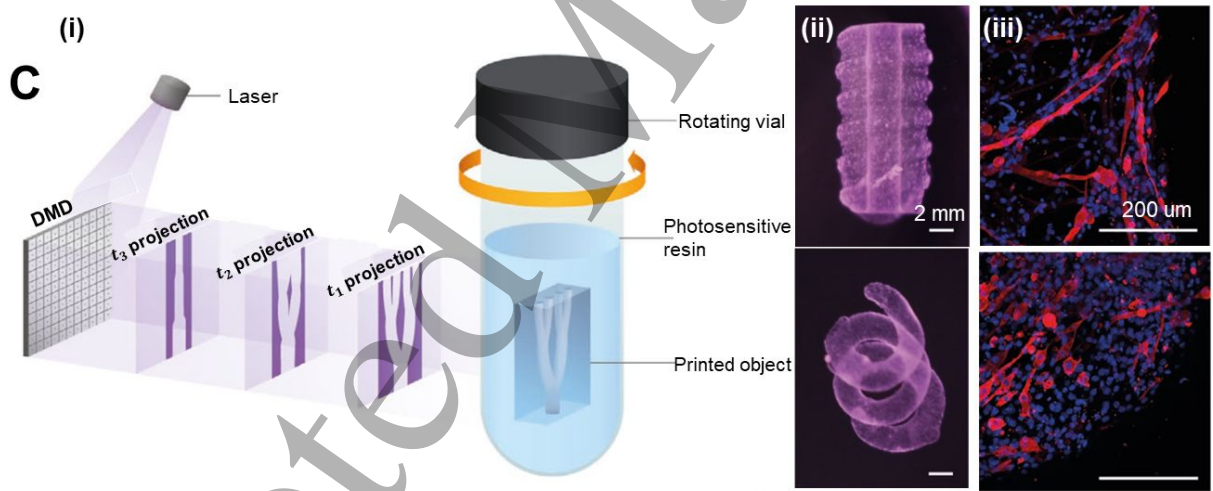
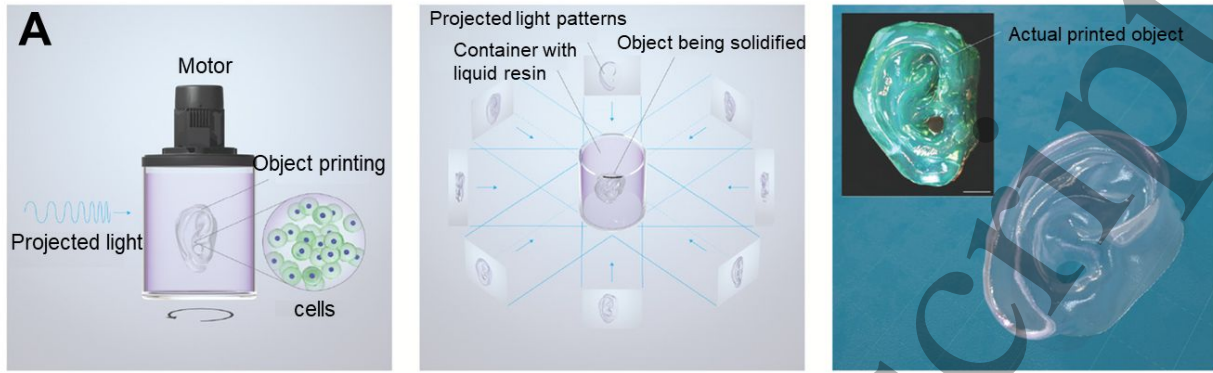


Figure 4. Improvement in VBP accuracy with an integrated feedback system. **(A)** Schematic of the data processing for a vessel model [41]. **(i)** Recording the background images of empty bottle (I_{bg}). **(ii)** Recording the images during printing (I_{rec}). **(iii)** Computing the difference of background images and printing images ($I_{diff} = I_{bg} - I_{rec}$). **(iv)** Setting the threshold of background images ($I_{thresh} = I_{diff} > T$). **(v)** Sorting the polymerization images by time. **(vi)** The recording images was back-projected in 3D to detect material in what time and position to solidify. **(vii)** Dose add or reduction in the next print depending on the solidify information of step **(vi)**. **(B)** The images were recorded by the camera at different time points corresponding to **(A)**. **(i)** The images of printing vial at the beginning. **(ii)** The images of resin printing. **(iii)** The different value images (I_{diff}). **(iv)** The images of the changes compared to the empty printing vial after setting the threshold. **(v)** The images of resin polymerization. **(vi)** Back-project polymerization times in 3D. **(vii)** Weighting method was applied to the intensity of each voxel based on the recorded polymerization. **(C)** The model of mouse pulmonary artery with and without feedback. **(D)** The

1
2
3 model of hearing aid with and without feedback. (B-D) Reproduced with permission [40].
4
5 Copyright 2020, Springer Nature Inc. VBP: Volumetric bioprinting.
6
7
8
9
10
11
12
13
14
15
16
17
18
19
20
21
22
23
24
25
26
27
28
29
30
31
32
33
34
35
36
37
38
39
40
41
42
43
44
45
46
47
48
49
50
51
52
53
54
55
56
57
58
59
60

Accepted Manuscript

1
2
3 photoresins under 405-nm wavelength light source. Reproduced with permission [39]. Copyright
4 2020, American Association for the Advancement of Science. (D) Synthesis of dual-colour
5 photoinitiator (DCPI). Reproduced with permission [42]. Copyright 2020, Springer Nature. (E)
6 Schematic of silicon carbide ceramics synthesis and printed structures. Reproduced with
7 permission [89]. Copyright 2022, Wiley-VCH GmbH Inc. SS: Silk sericin. SF: Silk fibroin. Ru:
8 Tris-bipyridyl-ruthenium (II) hexahydrate. SPS: Sodium persulfate.
9
10
11
12
13
14
15
16
17
18
19
20
21
22
23
24
25
26
27
28
29
30
31
32
33
34
35
36
37
38
39
40
41
42
43
44
45
46
47
48
49
50
51
52
53
54
55
56
57
58
59
60



1
2
3 **Figure 7.** Biomedical applications of VBP. (A) The cochlear model was volumetrically bioprinted
4 with a resin mixed with equine tissue samples and cells (stained with alcian blue to facilitate
5 visualization). Reproduced with permission [75]. Copyright 2019, Wiley-VCH GmbH Inc. (B)
6 Schematic of a hepatic organoid culture system, cells were isolated from human liver biopsies,
7 which were then dynamically cultured in a spinner flask system to establish high yields of hollow
8 epithelial organoid structures (microscopy image scale bar = 250 μm). Reproduced with
9 permission [77]. Copyright 2022, Wiley-VCH GmbH Inc. (C) (i) Schematic of volumetrically
10 printed a vessel branch model. (ii) Volumetrically bioprinted a C2C12-laden complex free-form
11 object. (iii) Immunofluorescence images of volumetrically bioprinted myotubes differentiation
12 after 3 weeks of culture (Myosin Heavy Chain: red, Nuclei: blue, scale bars: 200 μm). Reproduced
13 with permission [79]. Copyright 2021, Wiley-VCH GmbH Inc. (D) Volumetrically bioprinted SS
14 and SF constructs embedded with mouse myoblasts C2C12 cells. Reproduced with permission
15 [68]. Copyright 2023, Springer Nature. SS: Silk sericin, SF: Silk fibroin. C2C12: Mouse myoblasts.
16 VBP: Volumetric bioprinting.
17
18
19
20
21
22
23
24
25
26
27
28
29
30
31
32
33
34
35
36
37
38
39
40
41
42
43
44
45
46
47
48
49
50
51
52
53
54
55
56
57
58
59
60

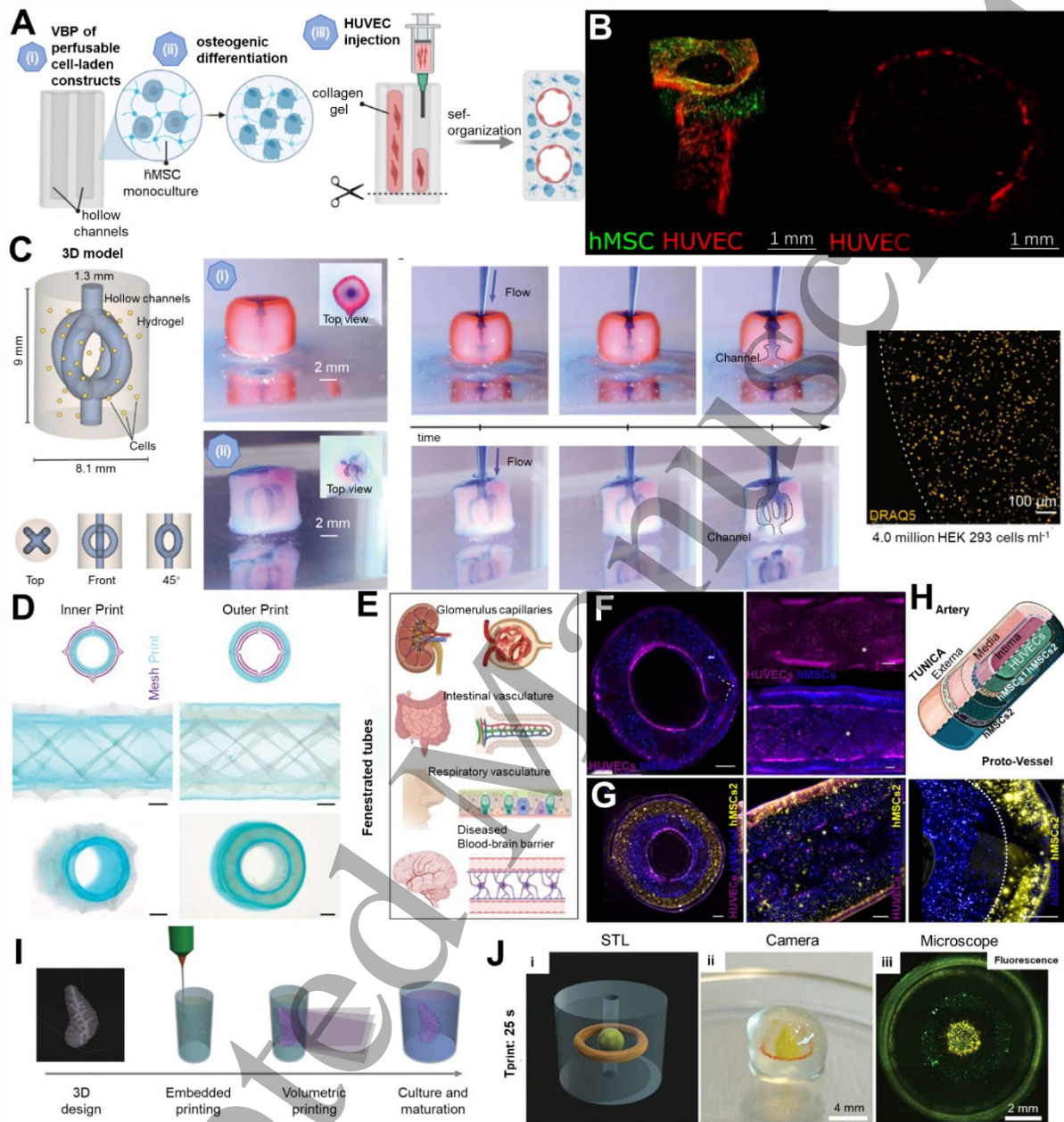


Figure 8. Biomedical applications of VBP. (A) (i) Volumetrically bioprinted hMSC-laden hollow pre-vascularization model and cultured for 6 d. (ii) The HUVECs suspension was injected into the hollow channels. (iii) Schematic of heterocellular perfusable pre-vascularization model after 14 d of culture. Reproduced with permission [80]. Copyright 2023, Wiley-VCH GmbH Inc. (B) The 3D confocal image of a hollow pre-vascularization model on 14 d of culture, hMSCs were stained with calcein-AM (green) and HUVECs were stained with DiD (red). Reproduced with permission [80]. Copyright 2023, Wiley-VCH GmbH Inc. (C) The scattering-corrected VBP method permits

1
2
3 printing complex hollow channels with high concentration bioink contained 4×10^6 human
4 embryonic kidney 293 cells mL^{-1} . **(i)** The blue dye couldn't pass through channels without
5 scattering correction. **(ii)** The blue dye could pass through channels using scattering corrected VBP.
6
7 Reproduced with permission [96]. Copyright 2023, Wiley-VCH GmbH Inc. **(D)** VBP across melt
8 electrowritten technology was successfully used to manufacture intricate, multi-material and
9 mechanical stability tubular structures, and could be used to volumetrically print structures inner
10 or outer of MEW mesh. Reproduced with permission [84]. Copyright 2023, Wiley-VCH GmbH
11 Inc. **(E)** VBP across melt electrowritten technology could be used to print various fenestrated
12 structures of native tissues/structures. Reproduced with permission [84]. Copyright 2023,
13 Wiley-VCH GmbH Inc. **(F)** Two-layer VBP across melt electrowritten technology could be used
14 to bioprint tubular constructs with hMSCs (blue) and HUVEC (magenta). Scale bar: 500 μm .
15 Reproduced with permission [84]. Copyright 2023, Wiley-VCH GmbH Inc. **(G)** Three-layer VBP
16 across melt electrowritten technology could be used to bioprint tubular construct hMSCs (blue and
17 yellow) and HUVEC (magenta). Scale bar: 500 μm . Reproduced with permission [84] Copyright
18 2023, Wiley-VCH GmbH Inc. **(H)** Schematic of proto-vessel. Reproduced with permission [84].
19 Copyright 2023, Wiley-VCH GmbH Inc. **(I)** Sequential of extrusion-VBP combined printing.
20 Reproduced with permission [78]. Copyright 2023, Wiley-VCH GmbH Inc. **(J)** VBP of complex
21 co-culture model. **(i)** STL file. **(ii)** Optical image of the printed structure. **(iii)** Microscope image
22 of the printed structure. Reproduced with permission [78]. Copyright 2023, Wiley-VCH GmbH
23 Inc. VBP : Volumetric bioprinting. hbMSCs: Human bone marrow-derived mesenchymal stromal
24 cells. HUVECs: Human umbilical vein endothelial cells. MEW: Melt electrowriting
25
26
27
28
29
30
31
32
33
34
35
36
37
38
39
40
41
42
43
44
45
46
47
48
49
50
51
52
53
54
55
56
57
58
59
60

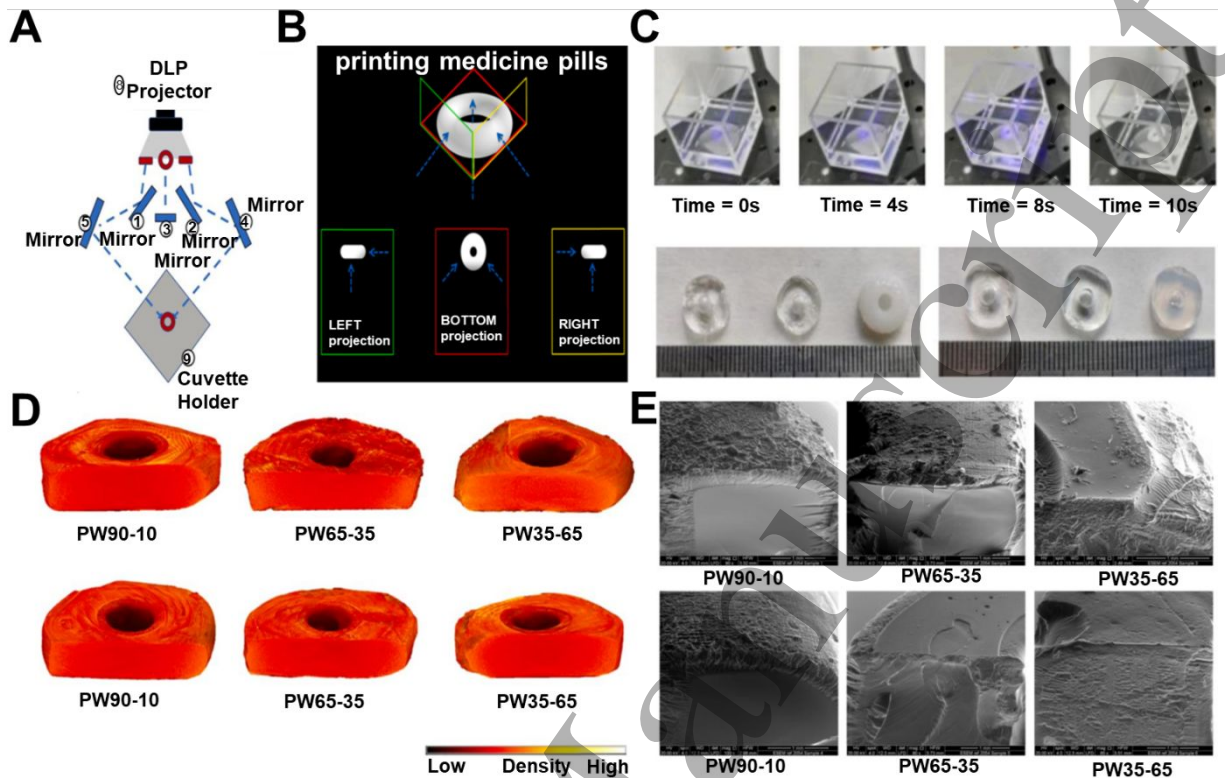


Figure 9. VBP of medicinal pills. (A) Schematic of VBP device. (B) Schematic of the irradiance of photosensitive resin with three orthogonal light beams. (C) Sequential view of the cuvette during the pill fabrication process. (D) X-ray micro-CT images of different pills. (E) Environmental scanning electron microscope (ESEM) images of cross sections of different printed pills. (A-E) Reproduced with permission [71]. Copyright 2022, Elsevier Inc. VBP: Volumetric bioprinting.

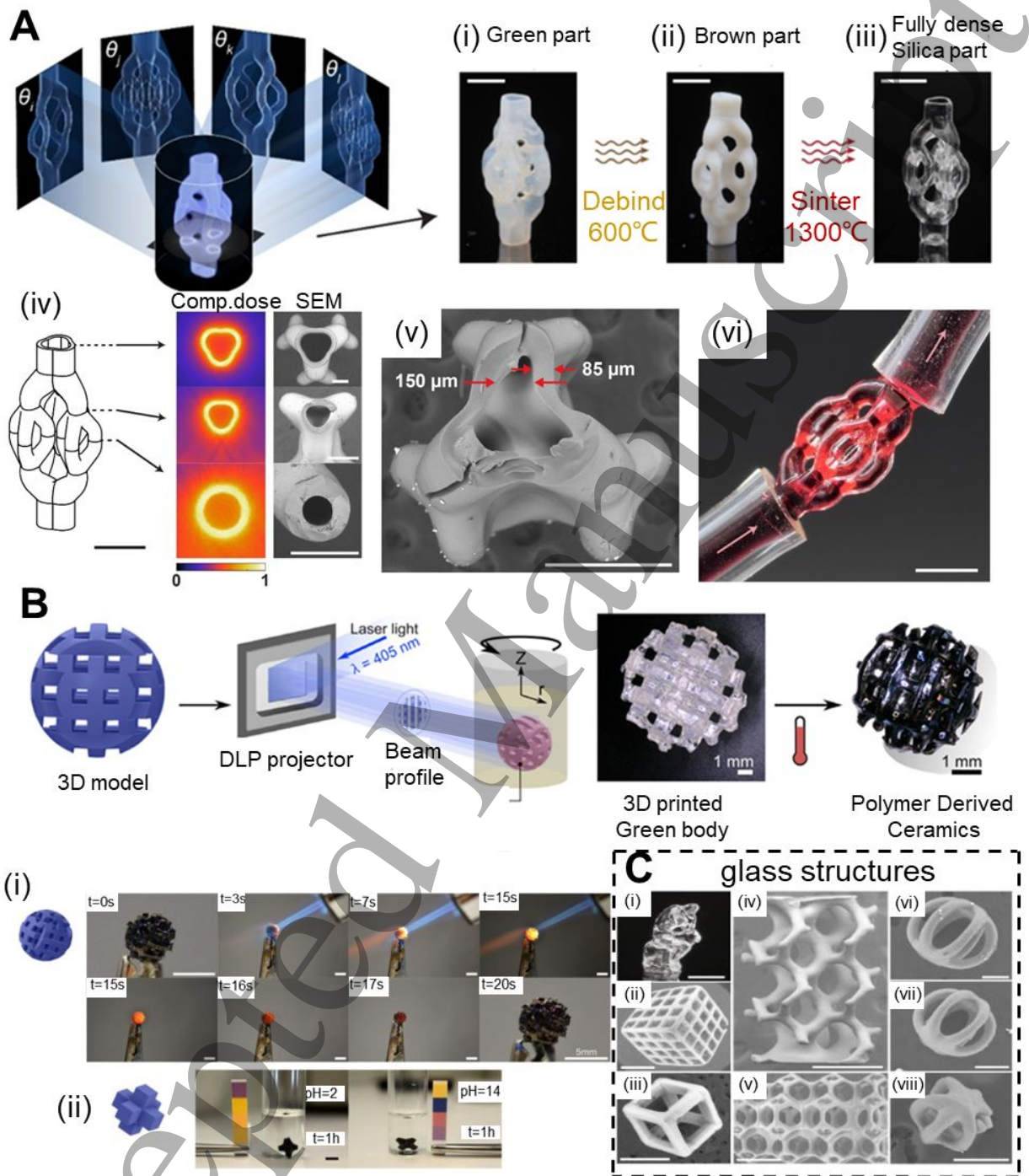


Figure 10. VBP of silicon glass and silicon oxycarbide ceramics. (A) VBP of glass. (i)-(iii) The resulting green parts were subjected to thermal treatment in two steps. Scale bar: 2 mm. (iv)-(v) The representative slices of trifurcated channel. (vi) Dye passes through the model channel. Scale bar: 2 mm [88]. (B) Volumetrically printed silicon oxycarbide ceramics, the 3D model of the desired part was used to calculate a set of light patterns, which were projected onto a rotating vial

1
2
3 filled with a photocurable preceramic resin. The resulting solid green body was retrieved from the
4 liquid resin, and pyrolyzed at $T = 1000^{\circ}\text{C}$. **(i)** Resistance of ceramic test with a butane torch
5 ($\approx 1400^{\circ}\text{C}$). **(ii)** Acid base test for 1 h. Reproduced with permission [89]. Copyright 2022,
6 Wiley-VCH GmbH Inc. **(C)** **(i)** Photograph of a ‘Thinker’. **(ii)** The scanning electron microscope
7 (SEM) micrograph of 4×4 cubic lattice. **(iii)** SEM micrograph of cubic structure. **(iv)** SEM
8 micrograph of skeletal gyroid lattice. **(v)** SEM micrograph of tetrakaidecahedron lattice. **(vi)** SEM
9 micrograph of spherical cage structure. Scale bars: **(i)-(v)** 1 mm, **(vi)** 200 μm . **(A)** and **(B)**
10
11
12
13
14
15
16
17
18
19
20
21
22
23
24
25
26
27
28
29
30
31
32
33
34
35
36
37
38
39
40
41
42
43
44
45
46
47
48
49
50
51
52
53
54
55
56
57
58
59
60

Reproduced with permission [88]. Copyright 2022, The American Association for the
Advancement of Science. VBP: Volumetric bioprinting.

Table1. List of abbreviations.

Abbreviation	Full name	Abbreviation	Full name
VBP	Volumetric bioprinting	GelMA	Gelatin methacryloyl
VAM	Volumetric additive manufacturing	BPAGDA	Bisphenol A glycerolate (1 glycerol/phenol) diacrylate
3DP	3D printing	PEGDA	Poly (ethylene glycol) diacrylate
FDM	Fused deposition modeling	CQ	Photoinitiator camphorquinone
SLA	Stereolithography	EDAB	Ethyl 4-dimethylaminobenzoate
SLS	Selective laser sintering	DCPI	Dual-colour photoinitiator
SLM	Selective laser melting	SiOC	Silicon oxycarbide
DLP	Digital-light processing	BDDA	1,4-butandiol-diacrylate
CLIP	Continuous liquid interface printing	TPO	Diphenyl-(2,4,6-trimethylbenzoyl)-phosphine oxide
iCLIP	Injection continuous liquid interface production	PCP	Pre-ceramic polymer
CAL	Computed axial lithography	PDC	Polymer-derived ceramic
UV	Ultraviolet	Gel-NB	Gelatin-norbornene
CT	Computed tomography	PEG4SH	4-arm-PEG-thiol
DMD	Digital micromirror device	DOTD	3,6-dioxa-1,8-octanedithiol
MEMS	Micro-electromechanical system	CA	Carbic anhydride
SLM	Spatial light modulators	C2C12	Mouse myoblasts
CGH	Computer-generated hologram	Micro-CAL	Microscale computed axial lithography
STL	Stereolithography	AI	Artificial intelligence
CAD	Computer Aided Design	ABS	Acrylonitrile Butadiene Styrene
DCP	Dual-colour photopolymerization	hbMSCs	Human bone marrow-derived mesenchymal stromal cells
LAP	Lithium phenyl-2,4,6-trimethylbenzoylphosphinate	GFP-HUVECs	Green fluorescent human umbilical vein endothelial cells
PI	Photoinitiator	MEW	Melt electrowriting
SS	Silk sericin	Co	Coinitiator
SF	Silk fibroin		

Table2. (Bio)inks investigated in volumetric printing.

Irradiation wavenumber (nm)	Monomers	Photoinitiator and co-initiator	Refs
525	Silk sericin	Tris-bipyridyl-ruthenium (II) hexahydrate, sodium persulfate;	[68]
525	Silk fibroin	Tris-bipyridyl-ruthenium (II) hexahydrate, sodium persulfate;	[68]
385	Poly(ethylene glycol) diacrylate;	Lithium phenyl-2,4,6-trimethylbenzoylphosphinate;	[70]
405	Gelatin;carbic anhydride;	Lithium phenyl(2,4,6-trimethylbenzoyl)phosphinate;	[75]
365	GelMA	Lithium phenyl(2,4,6-trimethylbenzoyl)phosphinate;	[77], [80]
Blue light at ~455; UV at~365	Glycerolate diacrylate; Poly(ethylene glycol) diacrylate;	Camphorquinone;- photoinitiator(PI); Ethyl 4-dimethylaminobenzoate;	[80]
532	Poly(ethylene glycol) diacrylate;	Irgacure 784;	[38]
405 blue color channel	Bisphenol A glycerolate (1' glycerol/phenol) diacrylate; Poly(ethylene glycol) diacrylate;	Camphorquinone; Ethyl 4-dimethylaminobenzoate;	[39]
405 green color channel	Gelatin methacrylate;	Tris(2,2bipyridyl)dichlororuthenium(II) hexahydrate; Sodium persulfate;	[39]
405	Di-pentaerythritol pentaacrylate;	Phenylbis(2,4,6-trimethylbenzoyl)phosphine oxide;	[41]
375	Pentaerythritol tetraacrylate;	5-Cyano-1,2,3,3-tetramethylindolenium iodide;	[42]
from 450 to 700;		4-Fluoro-3'-formyl-4'-hydroxybenzophenone;	
375;	Diurethane dimethacrylate;	5-Cyano-1,2,3,3-tetramethylindolenium iodide;	[42]
from 450 to 700;		4-Fluoro-3'-formyl-4'-hydroxybenzophenone;	
375;	Diurethane dimethacrylate;	5-Cyano-1,2,3,3-tetramethylindolenium iodide;	[42]
from 450to 700;	2-hydroxyethylmethacrylate;	4-Fluoro-3'-formyl-4'-hydroxybenzophenone;	

1				
2				
3	442	Trimethylolpropane ethoxylate	Camphorquinone;	[88]
4		triacrylate ;	Ethyl 4-(dimethylamino)benzoate;	
5		Hydroxyethylmethacrylate ;	2,2,6,6-tetramethyl-1-piperidinyloxy;	
6				
7	405	Polysiloxane;	Diphenyl-(2,4,6-trimethylbenzoyl)-phosphin oxide;	[89]
8		1,4-butandiol-diacrylate;		
9	405	Gelatin methacryloyl;	Lithium phenyl-2,4,6-trimethylbenzoylphosphinate;	[96]
10	405	Di-pentaerythritol pentaacrylate;	Phenylbis(2,4,6-trimethylbenzoyl)phosphine oxide;	[79]
11	405	Aliphatic urethane diacrylate;	Phenylbis(2,4,6-trimethylbenzoyl)phosphine oxide;	[79]
12	405	Vinyl-terminated PDMS 62 kg/mol;	Ethyl (2,4,6-trimethylbenzoyl)phenylphosphinate;	[84]
13		Fumed silica reinforced vinyl-		
14		terminated;		
15		(Mercaptopropyl)Methylsiloxane-		
16		dimethylsiloxane;		
17				
18	460	Bisphenol A glycerolate diacrylate;	Camphorquinone;	[96]
19		Poly(ethylene glycol) diacrylate;	Ethyl 4-dimethylaminobenzoate;	
20	405	Urethane dimethacrylate IPDI;	2-Methyl-4-(methylthio)2-morpholinopropiophenone;	[98]
21	405	Bisphenol A glycerolate diacrylate ;	Irgacure 907 ;	[100]
22		Poly(ethylene glycol) diacrylate ;	-Methyl-4'-(methylthio)-2-morpholinopropiophenone;	[99]
23				
24				
25	405	Tri-allyl isocyanurate;	Irgacure 907;	[100]
26		Tris[2-(3-	2,2,6,6-tetramethyl-1-piperidinyloxy;	
27		mercaptopropionyloxy)ethyl]		
28		isocyanurate;		
29				
30				
31				
32				
33				
34				
35				
36				
37				
38				
39				
40				
41				
42				
43				
44				
45				
46				
47				

Table3. Comparison of different bioprinting technologies.

Bioprinting technology	Advantages	Disadvantages	Applications	Refs
Extrusion	<ul style="list-style-type: none"> ● Suitable for heterogeneous tissue structures bioprinting ● Suitable for in situ and in vivo bioprinting 	<ul style="list-style-type: none"> ● Relative low printing speed (Minutes-hours) ● Relative low feature size resolution (>100 μm) ● Bioink needs suitable rheological properties 	<ul style="list-style-type: none"> ● Tissue engineering and spatially heterogeneous tissues bioprinting ● In situ bioprinting 	[11]-[17]
Inkjet	<ul style="list-style-type: none"> ● Low cost ● Easy to operation and develop 	<ul style="list-style-type: none"> ● Easy to clog ● Shear stress affects cell viability (70%-90%) 	<ul style="list-style-type: none"> ● Drug screening ● Drug-loaded vesicles ● Scaffold fabrication 	[6]-[9]
Vat photopolymerization	<p>DLP</p> <ul style="list-style-type: none"> ● High resolution features (10-50 μm) ● Possible to create geometrically complex constructs ● The ability to integrate multiple bioresins to printing heterogeneity constructs <p>VBP</p> <ul style="list-style-type: none"> ● Unprecedented printing speed (tens of seconds) ● High cell viability (>90%) ● Contactless printing ● Ultra-low concentration bioinks ● Possible to create geometrically complex constructs 	<ul style="list-style-type: none"> ● Use of UV light source ● Bioink must be photocrosslinkable ● Centimeter-scale constructs ● Relative low feature size resolution (30-500 μm) ● Deep light penetration 	<ul style="list-style-type: none"> ● Vascularized constructs ● Tissue models and cell-laden implants ● Complex constructs ● Organoids ● Scaffolds ● Vascularized constructs 	[21]-[26]

DLP: Digital-light processing. VBP: Volumetric bioprinting. UV: Ultraviolet.

Table4. The cell types used in VBP.

Cell type	Cell concentration	Cell viability	Printing time	Model	Resolution	Biomaterials	Refs
C2C12	5×10^6 cells mL ⁻¹	90% (14 d)	~45 s	Screw	~57 μ m	SF	[68]
C2C12	5×10^6 cells mL ⁻¹	250% (14 d)	~45 s	Screw	~45.9 μ m	SS	[68]
ACPCs	1×10^7 cells mL ⁻¹	>85% (7 d)	Seconds	Disc constructs	144.69 \pm 13.55 μ m	GelMA	[75]
Hepatic organoids	5×10^6 cells mL ⁻¹	93.3 \pm 1.4% (10d)	~20 s	Sphere	41.5 \pm 2.9 μ m	GelMA	[77]
C2C12	1×10^6 cells mL ⁻¹	90% (7 d)	Seconds	Spiral	~200 μ m	Gelatin-norbornene (Gel-NB)/PEG4SH	[79]
NHDF	1×10^6 cells mL ⁻¹	90% (7 d)	~10-11 s	Branch	~200 μ m	Gelatin-norbornene (Gel-NB)/PEG4SH	[79]
hMSC	3×10^6 cells mL ⁻¹	>90%	<60 s	Vascularization	micrometer-scale	GelMA	[80]
Human embryonic kidney 293	4×10^6 cells mL ⁻¹	~90%	Seconds	A construct with a core surrounded by four channels	~ 100 μ m	GelMA	[96]

C2C12: Mouse myoblasts. ACPCs: Articular chondroprogenitor cells. NHDF: Normal human dermal fibroblasts. hMSC: Human mesenchymal stem cells. SF: Silk fibroin. SS: Silk sericin. GelMA: Gelatin methacryloyl. PEG4SH: 4-arm-PEG-thio.